Proteomic analysis of the TDP-43-associated insoluble fraction from NEFH-TDP-43 mouse brain suggests sustained stress granule formation, CLUH granule recruitment and impaired mitochondrial metabolism

Felicity Dunlop [1], Shaun Mason[1], Stavroula Tsitkanou[2], Aaron P. Russell[1],

[1] Institute for Physical Activity and Nutrition, School of Exercise and Nutrition Sciences, Deakin University, Geelong, Australia

[2] Cachexia Research Laboratory, Exercise Science Research Center, Department of Health, Human Performance and Recreation, University of Arkansas, AR, USA

Correspondence
Dr Felicity Dunlop
Institute for Physical Activity and Nutrition, School of Exercise and Nutrition Sciences, Deakin University, Geelong, Australia
Email: f.dunlop@deakin.edu.au

Key words: Motor neuron disease, amyotrophic lateral sclerosis, TDP-43, stress granule, proteomics, CLUH

Abstract

Cytoplasmic accumulation and aggregation of TDP-43 is a hallmark of ~97% of ALS cases. Formation of TDP-43 insoluble aggregates is suggested to either directly or indirectly cause motor neurone loss and progressive neuromuscular degeneration, although how this occurs is not precisely understood. Cytoplasmic TDP-43 is observed in stress granules (SG). SGs are ribonucleoprotein (RNP) complexes formed during stress conditions, consisting of mRNAs and RNA-binding proteins (RNPs). Chronic TDP-43/SG formation may play a role in neuromuscular degeneration in ALS. The composition of *in vivo* TDP-43-asscociated SGs in ALS not known. This knowledge may provide insights into the molecular pathways impaired by TDP-43-associated SGs and suggest disease modifying mechanisms. The aim of this study was to isolate and analyse the proteome of the insoluble TDP-43-associated SG fraction from brain tissue of end-stage TDP-43ΔNLS mice. Proteomic analysis identified 134 enriched and 17 depleted proteins in the TDP-43ΔNLS mice, when compared to the control mice. Bioinformatics analyses of the impacted proteins from the SG preparation suggested that brain tissue from end-stage NEFH-TDP-43ΔNLS mice have sustained SG formation, CLUH granule recruitment and impaired mitochondrial metabolism. This is the first time that CLUH granule recruitment has been demonstrated in ALS and the known role of CLUH suggests that cell starvation is a potential mechanism of motor neurone loss that could be targeted in ALS.

Introduction

The NEFH-TDP-43ΔNLS mouse is a well-established model of amyotrophic lateral sclerosis (ALS). Disruption of the nuclear localisation sequence of the native human TDP-43 coding sequence results in cytoplasmic accumulation of TDP-43 in neuronal tissues (Walker et al., 2015), which is a hallmark of ~97% of ALS cases (Ling et al., 2013; Neumann et al., 2006). Cytoplasmic TDP-43 forms clumps of protein within the cell which characteristically pellet with centrifugation unless extracted by boiling in SDS first (Xiong et al., 2014). The insoluble aggregate results either directly or indirectly in motor neurone loss and progressive neuromuscular degeneration (Arai et al., 2006; Hergesheimer et al., 2019; Neumann et al., 2006). The intracellular aggregation of insoluble TDP-43 contributes to its broad and complex role in ALS as it impacts numerous processes within multiple compartments, including the nucleus, cytoplasm, mitochondria and neuromuscular junction (Lepine et al., 2022; Prasad et al., 2019; Wang et al., 2019). TDP-43 protein aggregation is theorised to occur via interaction of the intrinsically disordered c-terminal domain (Prasad et al., 2019; Santamaria et al., 2017) or via the phosphorylation of TDP-43 (Hasegawa et al., 2008; Inukai et al., 2008; Neumann et al., 2006); the latter influencing liquid-liquid phase separation and interaction with intracellular stress-related entities including stress granules (SG) (Colombrita et al., 2009).

SGs are membraneless ribonucleoprotein (RNP) complexes formed by the aggregation of mRNAs and RNA-binding proteins (RBPs) (Advani & Ivanov, 2019). SGs are formed during stress conditions and increase in size and number in response to stress (Kedersha et al., 2005; Ohn et al., 2008). Canonical SG formation is initiated by phosphorylation of eukaryotic initiation factor 2α (eif2α) by the 4 known stress specific kinases PERK (unfolded proteins), HRI (oxidative stress), GCN2 (starvation) or PKR (viral infection/cytoplasmic RNA) (Matsumiya et al., 2023). The physiological role of SGs is to protect cytoplasmic untranslated mRNAs and stalled pre-initiation complexes following acute stress by protein-protein and protein-RNA binding (Wolozin & Ivanov, 2019). These acute granules dissipate following stress removal. However, their chronic presence results in pathological cytoplasmic aggregates, that have been linked to ALS (Daigle et al., 2016). TDP-43 is a major architect in the development of physiological SGs and in pathological cytoplasmic aggregates in neurons of people with ALS and in other neurodegenerative conditions ALS (Fan & Leung, 2016; Prasad et al., 2019). TDP-43 contributes to SG development in neuronal tissue through its assembly with core RBPs such as T-Cell-Restricted Intracellular Antigen- (TIA-1), eukaryotic translation initiation factor (eIF3), polyadenylate-binding protein (PABP) and GTPase Activating Protein (SH3 Domain) Binding Protein (G3BP1) and 40S ribosomal subunits (Fan & Leung, 2016; Wolozin & Ivanov, 2019) and through the formation of amyloid-like aggregates (Prasad et al., 2019).

Our current understanding of formation, composition and potential role of SGs in ALS has come from cell culture studies (Asadi et al., 2021). Several studies have also performed histological analysis of post-mortem brain samples from ALS donors, identifying TDP-43 cytoplasmic inclusions colocalizing with SG markers, eIF3, G3PB1, PABP-1 and TIA-1 (Asadi et al., 2021; Liu-Yesucevitz et al., 2010). Attempts to determine the presence of TDP-43 in SG fractions isolated from tissues is limited and may lack specificity due to TDP-43 immunoprecipitation from soluble and not insoluble fractions (Montalbano et al., 2020). Proteomics analysis has been performed to observe changes in postmortem frozen motor cortex samples form ALS donors compared with healthy control samples (Lee et al., 2023) as well as longitudinal analysis in cortex samples from NEFH-TDP-43 mice (San Gil et al., 2024). These studies identified multiple disease-related changes in biological pathways. However, these analyses were performed using soluble protein fractions (Lee et al., 2023; San Gil et al., 2024) without TDP-43 immunoprecipitation, and would therefore not accurately capture the TDP-43-associated SG proteome.

Presently, the composition of TDP-43-associated SGs from *in vivo* models of ALS is lacking. Here, we prepared and analysed the proteome of the insoluble TDP-43-associated SG fraction from brain tissue of end-stage TDP-43ΔNLS mice. When compared with) control mice, 134 proteins were enriched and 17 were depleted in the SG fraction. Bioinformatics analyses of the impacted proteins suggested the brain tissue from end-stage TDP-43ΔNLS mice have sustained SG formation, CLUH granule recruitment and impaired mitochondrial metabolism.

Methods

Animals

Six hTDP-43ΔNLS transgenic (Tg) mice harbouring a doxycycline (DOX)-suppressible transgene to express human TDP-43 (hTDP-43) with a defective nuclear localization signal (hTDP-43ΔNLS) under the control of the human neurofilament heavy chain *NEFH* promoter and 7 age-matched control mice were used in this study. The NEFH-TDP-43 mice were produced by the inter-cross of C57/BL6 *NEFH*-tTA$^{+/-}$ mice and C57/BL6 *tetO*-hTDP-43ΔNLS$^{+/+}$ mice (Tsitkanou et al., 2022; Walker et al., 2015). All mice were maintained on DOX-enriched chow (200 mg/kg; Gordons Specialty Feeds, Bargo NSW) and genotyped when weaned (Walker et al., 2015). DOX-enriched chow was removed at 6 weeks of age to induce the transgene. Seven littermate single transgenic mice were used as healthy, control mice and remain unaffected with the removal of the DOX-enriched chow. Mice were humanely killed 5 weeks after disease initiation when they approach disease end-stage and were close to 20% body weight loss. Mice were maintained on 12 hours light/dark cycles at a temperature range of 18-24°C and humidity between 40-70%. At end-stage mice were humanely killed by CO_2 asphyxiation. Brains were

immediately removed and snap frozen in liquid nitrogen and stored at –80°C until required. The study was approved by the Deakin University Animal Ethics Committee (G21-2020).

Immunoprecipitation and Western Blotting

For the initial antibody titration experiment, RIPA brain tissue extracts were prepared as previously described (Tsitkanou et al., 2022). Each IP (immunoprecipitation) contained 100 µg of RIPA extracted protein that was precleared with protein G magnetic beads.

Preclearing lysates with Protein G magnetic beads: Protein G magnetic beads (10 µl per sample) were washed with 300 µl modified RIPA buffer (50 mM Tris-HCl, pH 7.4, 150 mM NaCl, 0.25% deoxycholic acid, 1% NP-40, 1 mM EDTA, Millpore cat# 20-188) + 1:100 HALT Protease and Phosphatase inhibitors (cat# 78438, Pierce)) for 5 minutes on a rotating wheel at 4°C in individual 1.5 ml Eppendorf tubes. The washed beads were then placed on a magnetic rack (cat# 12321D, Invitrogen) to remove wash buffer. RIPA buffer and RIPA brain lysate (100 µg in a 300 µl final volume) were added to the beads. Following this 10 ul of 6% BSA was added and mixed on a rotating wheel at 4°C for 1-2 hours.

Immunoprecipitation: The precleared lysates were transferred to fresh 1.5 ml Eppendorf tubes containing 20 µl RIPA washed Protein G magnetic beads and 0.5, 1.0, or 2.0 µg of mouse IgG1 anti-human TDP-43 antibody (ProteinTech cat# 60019-2-Ig) was then added to each tube. The samples were placed on a rotating wheel overnight at 4°C. The following day samples were placed on magnetic rack for 2 minute to allow for bead binding. The supernatant was removed, and the beads washed a total of five times (Thomas et al., 1998). Beads were washed 2 x with wash buffer I (50 mM Tris-HCl, pH 7.5, 150 mM NaCl, 1% Triton X-100, 0.5% sodium deoxycholate), + inhibitors (cat# 78438, Pierce) 2 x with wash buffer II (50 mM Tris-HCl, pH 7.5, 500 mM NaCl, 0.1% Triton X-100, 0.05% sodium deoxycholate) and 1 x with wash buffer III (50 mM Tris-HCl, pH 7.5, 0.1% Triton X-100, 0.05% sodium deoxycholate). Samples for Western blotting were resuspended in 15 µl Urea-based SDS sample buffer (62.5 mM Tris-HCl, pH 6.8, 2% SDS, 10%-mercaptoethanol (vol/vol), 6 M urea, 20% glycerol), (Thomas et al., 1998) and heated at 95°C for 5 minutes. 30µg of RIPA lysate (starting material was included as a Western blot positive control) and samples were resolved on 4-15% Criterion Stain free gels (cat# 5678085 Biorad) at 200 Volts, 40 minutes. Proteins were transferred to a PVDF membrane by Western blotting at 100 volts for 1 hour. Membranes were blocked in 5% BSA in PBS at room temperature for 1 hour before overnight incubation with primary antibody mhTDP-43 (rabbit; Cat#10782-2-AP; 1:1000; ProteinTech). Blots were washed 3 times in TBST (20 mM TRIS, 150 mM NaCl, 0.1% w/v Tween® 20 detergent) for 10 minutes each. Donkey anti-mouse AlexaFluor 800 IgG antibodies (Life Technologies) diluted at 1:10,000 in 5% BSA in PBS was used as the secondary antibody with incubation at room

temperature for 1 hour. Blots were washed twice in TBST and once in PBS and then imaged using the infrared imaging system (Li-COR Biosciences, Lincoln, NE, USA).

Formaldehyde crosslinking and tissue lysis

Formaldehyde crosslinking and homogenization of brain tissue was adapted from previous protocols (Liu-Yesucevitz et al., 2010; San Gil et al., 2024; Sap et al., 2021). 500 µl of 0.5% formaldehyde in PBS was added to 30 mg of frozen mouse brain tissue, previously crushed under N_2 and placed on a rotating wheel for 10 mins at room temperature. Samples were then centrifuged at 6000 g for 15 seconds followed by removal of formaldehyde. To quench crosslinking, 500 µl of 250mM Tris-HCl pH 7.5 was added to the sample and gently mixed by pipetting for 45 seconds using wide bore pipette tips. The samples were then pelleted at 6000 g for 15 seconds followed by removal of Tris. 500 µl of ice-cold Co-IP buffer (20 mM Tris-HCL pH 7.5, 150 mM NaCl, 1 mM EDTA, 1% Triton X-100 + protease and phosphatase inhibitors) was then added to the pellet and placed on ice. Five 1.4mm Precellys beads (Bertin Instruments, Montigny-le-Bretonneux France) were added to each tube followed by homogenisation (Precellys bead homogeniser + CryoLys; Bertin Instruments, Montigny-le-Bretonneux, France) at 6000 rpm for 30 seconds each, with liquid N_2 cooling to 4°C. Following this, the samples were de-foamed in a CentriVap (Labconco, Kansas, USA) for 15 seconds. The homogenisation and de-foaming steps were repeated 5 times. The samples were then placed on rotating wheel for 1 hour at 4°C.

Stress Granule Enrichment

Stress granule enrichment was based on previous protocols (Jain et al., 2016; Wheeler et al., 2017). Following lysis the samples were centrifuged at 1000g for 5 min at 4°C with the supernatant then decanted into a 1.5 ml Eppendorf tube and the pellet discarded as cellular debris. The supernatant was then centrifuged at 18,000 g for 20 min at 4°C. The stress granule (SG) pellet was resuspended in 500 µl Co-IP buffer and centrifuged again at 18,000 g 20 min at 4°C. The SG pellet was again resuspended in 500 µl Co-IP buffer. A 5 µl aliquot was removed and used to determine protein concentration in triplicate using the BCA assay (Cat# 23225, Pierce). The remaining SG sample was kept on wet ice until required for immunoprecipitation.

TIA-1 and TDP-43 Immunoprecipitation of Crosslinked Samples

Bead washing and preclearing was conducted the same as for the non-cross-linked (native) samples above, with 10 µl of protein G magnetic beads per sample. Co-IP buffer was used in place of RIPA

buffer and 150 µg stress granule lysate was used. Immunoprecipitation was conducted the same as for native samples with 2.0 µg of either mouse IgG1 anti-human TDP-43 antibody (ProteinTech cat# 60019-2-Ig) or TIA-1 (Santa Cruz cat#1751) used for each overnight immunoprecipitation. Following the immunoprecipitation samples were washed using high stringency "SAP" wash buffers adapted from (Sap et al., 2021). Beads were washed 2 x with wash buffer I + inhibitors (50mM Tris pH 7.4; 300mM NaCl; 1mM EDTA; 0.1% Triton X-100), 1 x with wash buffer I (no inhibitors) and 1 x with wash buffer II (50mM Tris pH 7.4; 150mM NaCl; 1mM EDTA; 0.01% Triton X-100). Western blotting of crosslinked samples was conducted the same as for native samples but with samples heated at 100°C for 20 minutes in urea-based SDS sample buffer to reverse the crosslinking prior to SDS-PAGE.

Sample Preparation for Proteomics

SAP washed beads of immunoprecipitated samples for proteomics analysis were resuspended in 90 µl 2% SDS, 62.5 mM Tris-HCl (pH 6.8)(Sap et al., 2021). Following this 1.8 µl of 0.5 M TCEP (cat #C4706) and 8 µl 0.5 M IAA (cat #I6125) were added separately to the resuspended beads. Single step formaldehyde crosslinking reversal and disulfide bond reduction and alkylation was then done by heating the samples at 100°C for 30 minutes in the dark. The samples were cooled on ice and then placed on the magnetic rack for 2 minutes before the eluted proteins were transferred to a fresh 1.5ml tube and the spent beads discarded.

SP3 and Trypsin digestion: The eluted proteins were prepared for trypsin digestion using SP3 single-pot, solid phase enhanced protocol (Hughes et al., 2019). 5 mg of each Sera-Mag Hydrophilic and Hydrophobic magnetic SpeedBeads (Cytiva, cat. no. 45152105050250, cat. no. 65152105050250) were combined and washed with 1 ml LC-MS water (cat #1.15333) on a magnetic rack. Washed beads were resuspended in 1 ml LC-MS water and 20 µl added to each tube of eluted proteins. Binding of the proteins to the beads was induced with 120 µl of absolute ethanol (cat #459836) and mixed using a Thermomixer (Eppendorf, Macquarie Park, Australia) at 1600 rpm for 8 minutes. The bead bound proteins were washed three times with 80 % ethanol before resuspension in 60 µl digestion buffer (10% TFE, 100 mM HEPES pH 7.3) and 0.1 µg trypsin (cat #) and incubated for 18 hours at 37°C, 1200 rpm using a Thermomixer.

STAGE tips: Overnight trypsin digests were desalted using STAGE tips prepared from 2 layers of SDP-RPS membrane (Cat # 2341 Empore). The STAGE tips were first equilibrated in 50 µl each of acetonitrile (Cat #1.00029), 0.2 % TFA (Cat# T0699) in 30% methanol (cat #1.06035), and then 0.2% TFA by centrifugation at 500 g for 3 minutes each. Overnight trypsin digests were placed on the magnetic

rack. The supernatant containing the digested peptides were pipetted on top of equilibrated STAGE tip containing 150 µl 1 % TFA and centrifuged at 1000 g for 8 minutes. Tips were washed twice with 100 µl 0.2% TFA and once with 40 µl 1% TFA in 90% isopropanol by centrifugation at 1000 g for 5 minutes. Peptides were eluted into a fresh 1.5 ml tube with 60 µl 5 % ammonium hydroxide (cat # 221228) in 80 % acetonitrile and centrifuged at 1000 g for 3 minutes. Eluted peptides were dried in a CentriVap (Labconco, Kansas, USA) at 45°C for 30 minutes until dry and stored at 4°C. Peptides were resuspended in 20 µl loading buffer (2% (v/v) acetonitrile, 0.1% (v/v) TFA) for mass spectrometry analysis.

Liquid chromatography mass spectrometry

Samples were analyzed using an UltiMate 3000 RSLCnano (ThermoFisher Scientific) linked to an Orbitrap Exploris™ 240 Mass Spectrometer (ThermoFisher Scientific). Six microlitres of sample was loaded onto a PepMap 100 C18 (20 mm x 0.1mm, 5µm) nanoViper trap column for 3 mins at a flow rate of 15 µL/min with 2% (v/v) acetonitrile, 0.1% (v/v) TFA, and then resolved on a PepMap Neo C18 (75 µm x 500 mm, 2µm) nanoViper analytical column at a flow rate of 250 nL/min. Mobile phases consisted of 0.1% (v/v) Formic acid (A) and 80% (v/v) Acetonitrile/0.1% (v/v) Formic acid (B). Gradient conditions were: 0-2 min 2.5% B, 2-2.1 min 8% B, 2.1-122 min 32% B, 122-125 min 45% B, 125-133 min 99% B, 133-150 min 2.5% B. The column compartment was set at 50°C. Ion source conditions were: NSI type, static spray voltage, 2000V positive ion, 1500V negative ion, 275°C ion transfer tube temperature. MS1 data were acquired over 350-1200 m/z with an orbitrap resolution of 120000, RF lens 70%, and positive polarity. Dynamic exclusion was for 20s, with mass tolerances of 10 ppm. Data dependent analysis used a 3 s cycle time with HCD collision energy set at 30%. MS2 spectra were acquired with a fixed first m/z of 120 with an orbitrap resolution of 15 000.

Data analysis

Data were processed using Thermo Proteome Discover (v.3.0) with Sequest HT as the database search algorithm against the *Mus musculus* FASTA file (Uniprot). Input data to Sequest HT were as follows: Maximum missed tryptic cleavages 2, precursor mass tolerance 10 ppm, fragment mass tolerance 0.02 Da. Dynamic modifications were oxidation (methionine), and static modifications were carbamidomethylation (cysteine). The processing workflow also had the Percolator node used, with strict target FDR set at 0.01 and relaxed FDR set at 0.05. The target/decoy strategy was concatenated with validation based on the q-value. Data Normalization based on total peptide amount was used to

compensate for sample-to-sample variation. Protein abundances were calculated on the basis of summed peptide abundances of unique and razor peptides.

A complete list of all the TDP-43 associated proteins was generated by selection of all proteins that had quantifiable protein abundances in the TDP-43 sample group based on the unique accession numbers of the master protein. The gene symbols were used for cross species comparison against the Lunenfield RNA granule database and specific stress granule lists from (Jain et al., 2016) and (Hu et al., 2023). Protein ratios were calculated using protein abundances and Hypothesis testing was based on ANOVA (individual protein) calculations. Fold change individual protein ratios TDP-43/WT of >1.5 (Log2=0.58) and ANOVA p-value <0.05 were used as statistical cutoffs to determine significance and no imputation was used.

Protein-protein interactions, GO terms and Reactome pathways were identified using STRINGS (https://string-db.org/). A CLUH target list was generated by combining the data from (Gao et al., 2014) and (Schatton et al., 2017). All 256 proteins were retrieved from Table S3 (Guo et al., 2017) and 167 proteins were retrieved by sorting Table S1 data for Log2 Ratio KO/WT >0.58 and p-value <0.05 from Schatton *et al* (Schatton et al., 2017). The lists were combined as gene symbols to allow for comparison with both mouse and human proteins. Duplicates removed to provide a final list of 371 unique CLUH target proteins.

Supplemental Table S6 (file mmc6) was retrieved from (Guise et al., 2024) and the results sorted for p-value <0.05, Log2(FC)<0.58 for ALSvsCTL. The dataset described as “decreased early and late” was set to “true” to retrieve 540 consistently depleted proteins. The 41467_2021_27221_MOESM5_ESM file from (Altman et al., 2021) containing 249 depleted proteins was accessed and the gene symbol and corresponding accession numbers for the Log2FC<-1 246 proteins were retrieved (3 entries were removed as they were incomplete). Gene symbols were mapped to unique accession numbers using the Uniprot ID mapping function (https://www.uniprot.org/id-mapping) to prevent ambiguity. Mitochondrial proteins from the Guise *et al* dataset were then identified by comparison with the human mitochondrial database (Human MitoCarta3.0: 1136 mitochondrial genes: https://personal.broadinstitute.org/scalvo/MitoCarta3.0/human.mitocarta3.0.html) using the unique accession numbers. The same identification method was used for the Altman *et al* dataset however comparison was made with the mouse mitochondrial database (Mouse MitoCarta3.0: 1140 mitochondrial genes:

https://personal.broadinstitute.org/scalvo/MitoCarta3.0/mouse.mitocarta3.0.html). Both datasets were also checked against the CLUH target list. The CLUH target proteins from both datasets were then submitted to the STRINGS database as accession numbers for Reactome Analysis. The same significant Reactome pathways identified by our enriched insoluble SG fraction were used to colour a STRINGS diagram.

Results

The specificity of our immunoprecipitation (IP) with the TDP-43 antibody recognizing the human isoform (hTDP-43) is shown in Figure 1A. A TDP-43 IP was performed on RIPA lysates from crushed brain tissue from the NEFH-TDP-43 and Control mice. This was performed using increasing amounts of the hTDP-43 antibody (0.5, 1.0 and 2.0 µg). The IP samples were then probed using a TDP-43 antibody recognizing both the mouse and the human isoforms (mhTDP-43). RIPA extracted lysates (30 µg starting material) from the NEFH-TDP-43 and control mice were used as positive control samples. A band was detected in the RIPA extracted lysate from the NEFH-TDP-43 and control mice when using the mhTDP-43 antibody. Although 30 µg of protein was loaded for each sample, the band was stronger from the NEFH-TDP-43 brain due to the sample containing both the exogenous human and endogenous mouse TDP-43 proteins. The control mouse brain sample only contains the endogenous mouse TDP-43 protein. Probing the brain IP hTDP-43 samples with the mhTDP-43 antibody revealed an increasing signal with increasing amounts of the IP antibody for the NEFH-TDP-43 mice. No signal was detected in the control mouse, which is to be expected as the control mouse does not have the human TDP-43 protein present. Figure 1B shows the equal protein loaded for the RIPA lysates, as well as the IgG Heavy and Light Chains from the IP, showing the amounts of antibody loaded.

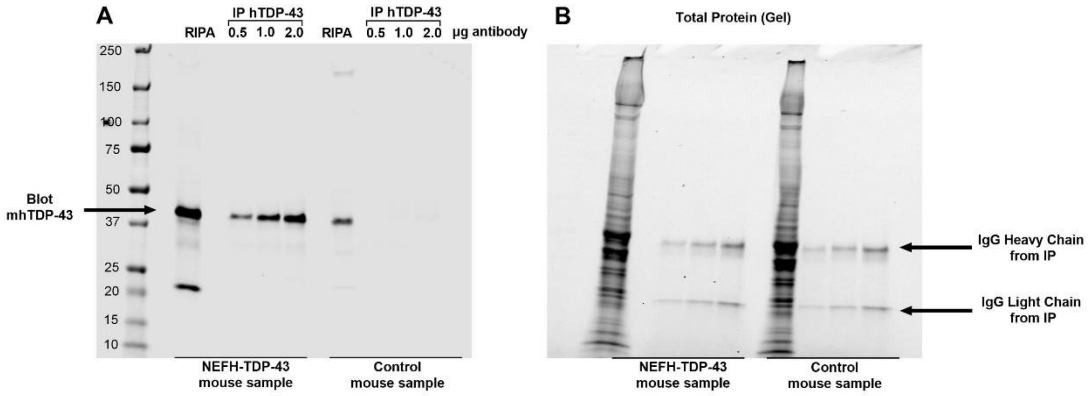

Figure 1. Establishing immunoprecipitation (IP) specificity using the TDP-43 antibody recognizing the human isoform (hTDP-43). (A) TDP-43 IP was performed on RIPA extracts of crushed brain tissue from the NEFH-TDP-43 and control mice using increasing amounts of the hTDP-43 antibody (0.5, 1.0 and 2.0 µg). The IP samples were then probed using a TDP-43 antibody recognizing both the mouse and the human isoforms (mhTDP-43). RIPA extracted starting material from the NEFH-TDP-43 and control mice were used as positive control samples. (B) Protein loading gel indicating equal protein loaded for the RIPA lysates, as well as evidence of increasing amounts of antibody used as shown by the IgG Heavy and Light Chains from the IP.

IP was performed with and without crosslinking, demonstrating that crosslinking is required to maintain protein-protein interactions within our SG preparation from brain tissue (Figure 2). IP of the SG preparation was performed with a TIA-1 antibody, as TIA-1 is a known SG core protein (Kedersha et al., 2000) and binds TDP-43 (McDonald et al., 2011). The samples were then probed with the antibody recognising both the mouse and human forms of the TDP-43 protein (mhTDP-43). Figure 2A shows that after crosslinking brain samples from control and NEFH-TDP43 mice, followed by TIA1 IP, TDP-43 is detected via western blotting in the NEFH-TDP-43, but not the control sample (compare lanes 2 and 3). When cross linking is not performed prior to TIA-1 IP, TDP-43 is not detected in the NEFH-TDP-43 sample (lane 5), indicating the loss of the protein-protein interaction. Additionally, IP was performed with and without crosslinking using the antibody that recognises the human TDP-43 isoform (hTDP-43), followed by probing with the mhTDP-43 antibody. TDP-43 was detected in the NEFH-TDP-43 samples only (compare lanes 6 and 7) and was not influenced by crosslinking (compare lanes 8 and 9). This demonstrates that the crosslinking process does not disrupt the epitope for the hTDP-43 antibody.

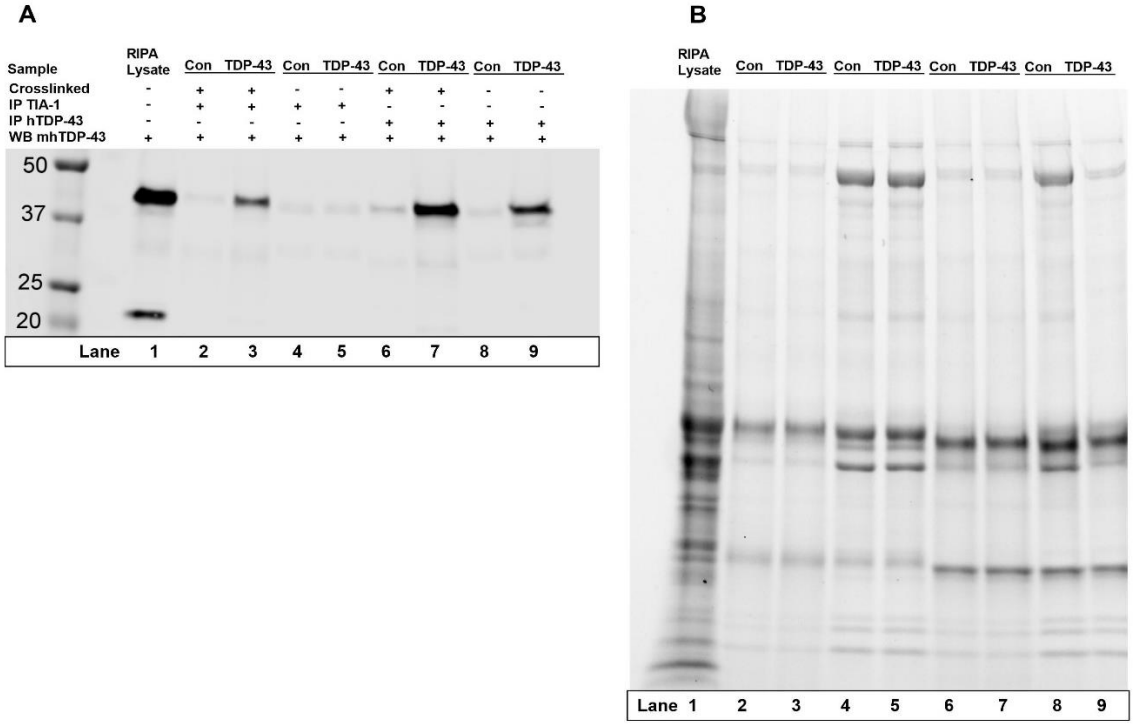

Figure 2. Immunoprecipitation (IP) with and without crosslinking using either TIA1 or TDP-43 antibodies. (A) IP of the SG preparation with a TIA1 antibody indicated that crosslinking is required to maintain protein-protein interactions within our SG preparation. IP of the SG preparation with the hTDP-43 antibody indicated that crosslinking does not disrupt the epitope for the hTDP-43 antibody. (B) Protein loading for all samples. Con, control mice; TDP-43, NEFH-TDP-43 mice.

Following LC-MS analysis of the TDP-43-associated SG fractions, 4,700 quantifiable proteins were identified (Supplementary Table 1). These proteins were compared against the RNA granule database (Millar et al., 2023). Of the 4,700 quantifiable proteins 2512 were identified as SG and RNA binding proteins (RBPs). Additionally, our proteins were compared against the mammalian SG proteome list of 540 proteins (Jain et al., 2016). From our list 383 proteins were found to be known SG marker proteins including the canonical SG initiator eIF2α, and several core SG proteins TIA-1, G3BP1, G3BP2, PABPC1 and CAPRIN1. Of the 4700 proteins, 134 proteins were significantly enriched while 17 proteins were significantly depleted, in the brain tissue from the NEFH-TDP-43 mouse brains, when compared to the control mice (TDP-43/control = fold change >1.5, $p<0.05$) (Supplementary Table 2). Figure 3 is a representative volcano plot showing the enriched proteins in red and the depleted proteins in green. Following comparison with the mammalian SG proteome (Jain et al., 2016), 24 of our 134 enriched proteins were known SG markers (Supplementary Table 2). Further comparison against a list of early and late stress granules markers (Hu et al., 2023) identified a further 16 SG markers, of which most were categorised as late SG markers. Therefore, 30% (40/134 proteins) of our SG preparation consisted of known SG markers (Hu et al., 2023; Jain et al., 2016). There were 17 proteins comparatively depleted in the SG fraction from the NEFH-TDP-43 mouse brains, when compared to the control mice (control/TDP = fold change >1.5, $p<0.05$) (Supplementary Table 3). Fourteen (82%) of these depleted proteins were associated with STRINGS keyword analysis *Phosphoprotein* (KW-05 97). KEGG Pathways relating to the depleted proteins included Calcium Signalling (mmu04020), MAPK Signalling (mmu04010) and NF-Kappa B Signalling (mmu04064).

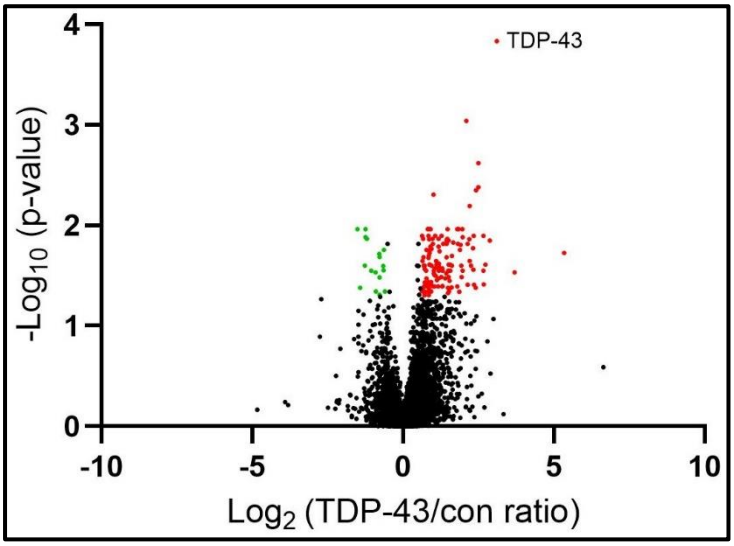

Figure 3. A volcano plot highlighting the enriched (red) and depleted (green) proteins in the TDP-43-associated insoluble SG fraction isolated from the brain tissue of end-stage NEFH-TDP-43 mice. The TDP-43 protein is specifically highlighted to shows its enrichment.

The 134 enriched proteins were entered into the STRINGS database to better understand their potential role in ALS pathogenesis (Figure 4). Overall, 70 % of the proteins could be categorised into just five GO terms including RNA binding shown in green (GO:0003723), ATP binding shown in purple (GO:0005524), ribose phosphate metabolic process shown in red (GO:0019693), mitochondrion shown in pink (GO:0005739) and cytoskeleton shown in yellow (GO:0005856).

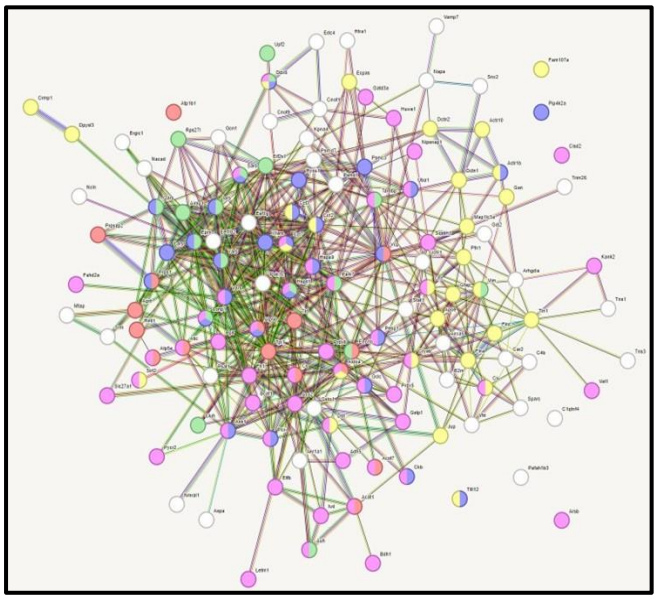

Figure 4. STRINGS pathway representation of the interaction between the 134 proteins enriched in the SG preparation from brain tissue of the end-stage NEFH-TDP-43 mice. Of the 134 proteins identified 70 % of these could be categorised into just five GO terms including ATP binding (purple), RNA binding (green), cytoskeleton (yellow), ribose phosphate metabolic process (red) and mitochondrion (pink).

The strength and false discovery rate of the categorized proteins are shown in Table 1.

Table 1. The strength and false discovery rate of the proteins categorized into the five GO terms.

Gene Ontology	Description	Strength	False discovery rate	Colour code
GO:0005524	ATP binding	0.5	9.59e-06	
GO:0003723	RNA binding	0.4	0.0326	
GO:0005856	Cytoskeleton	0.29	0.0146	
GO:0019693	Ribose phosphate metabolic process	0.79	6.83e-06	
GO:0005739	Mitochondrion	0.63	6.00e-17	

Of the 134 proteins, two proteins were localised exclusively to the nucleus, (Kpna1, Polr1c) and six were exclusively secreted proteins (Apoe, B2m, C1qtnf4, C4b, Sparc, and Vtn), as based on the uniprot entry. The GO term "mitochondrion" (GO:0005739) included 51/134 proteins. These 51 proteins were cross checked with the mitochondrial proteome (Morgenstern et al., 2021) and the Uniprot data base (https://www.uniprot.org/), indicating that 21 proteins were exclusively located to the mitochondria (Table 2). One of the proteins identified was the mRNA binding protein Clustered mitochondrial protein homologue (CLUH). It is noteworthy that 18 of the 21 mitochondrial proteins enriched were known CLUH targets (Table 2).

Table 2. The 21 proteins exclusively located to the mitochondria

Accession	Entry Name	Gene Names (primary)	Cluh target	Gene Names	Protein names
P99029	PRDX5_MOUSE	Prdx5	-	Prdx5 Prdx6	Peroxiredoxin-5, mitochondrial (EC 1.11.1.24) (Antioxidant enzyme B166) (AOEB166) (Liver tissue 2D-page spot 2D-0014IV) (PLP) (Peroxiredoxin V) (Prx-V) (Peroxisomal antioxidant enzyme) (Thioredoxin peroxidase PMP20) (Thioredoxin-dependent peroxiredoxin 5)
Q3TC72	FAHD2_MOUSE	Fahd2	-	Fahd2 Fahd2a	Fumarylacetoacetate hydrolase domain-containing protein 2A (EC 3.-.-.-)
Q9CZU6	CISY_MOUSE	Cs	-	Cs	Citrate synthase, mitochondrial (EC 2.3.3.1) (Citrate (Si)-synthase)
Q9D172	GAL3A_MOUSE	Gatd3	+	Gatd3 D10Jhu81e Gatd3a	Glutamine amidotransferase-like class 1 domain-containing protein 3, mitochondrial
O55125	NIPS1_MOUSE	Nipsnap1	+	Nipsnap1	Protein NipSnap homolog 1 (NipSnap1)
P63038	CH60_MOUSE	Hspd1	+	Hspd1 Hsp60	60 kDa heat shock protein, mitochondrial (EC 5.6.1.7) (60 kDa chaperonin) (Chaperonin 60) (CPN60) (HSP-65) (Heat shock protein 60) (HSP-60) (Hsp60) (Mitochondrial matrix protein P1)
Q99KI0	ACON_MOUSE	Aco2	+	Aco2	Aconitate hydratase, mitochondrial (Aconitase) (EC 4.2.1.3) (Citrate hydro-lyase)
P97807	FUMH_MOUSE	Fh	+	Fh Fh1	Fumarate hydratase, mitochondrial (Fumarase) (EC 4.2.1.2) (EF-3)
P56480	ATPB_MOUSE	Atp5f1b	+	Atp5f1b Atp5b	ATP synthase subunit beta, mitochondrial (EC 7.1.2.2) (ATP synthase F1 subunit beta)
P53395	ODB2_MOUSE	Dbt	+	Dbt	Lipoamide acyltransferase component of branched-chain alpha-keto acid dehydrogenase complex, mitochondrial (EC 2.3.1.168) (Branched-chain alpha-keto acid dehydrogenase complex component E2) (BCKAD-E2) (BCKADE2) (Dihydrolipoamide acetyltransferase component of branched-chain alpha-keto acid dehydrogenase complex) (Dihydrolipoamide branched chain transacylase) (Dihydrolipoyllysine-residue (2-methylpropanoyl)transferase)
Q9JHI5	IVD_MOUSE	Ivd	+	Ivd	Isovaleryl-CoA dehydrogenase, mitochondrial (IVD) (EC 1.3.8.4) (Butyryl-CoA dehydrogenase) (EC 1.3.8.1)
P56382	ATP5E_MOUSE	Atp5f1e	+	Atp5f1e Atp5e	ATP synthase subunit epsilon, mitochondrial (ATPase subunit epsilon) (ATP synthase F1 subunit epsilon)
Q80XN0	BDH_MOUSE	Bdh1	+	Bdh1 Bdh	D-beta-hydroxybutyrate dehydrogenase, mitochondrial (EC 1.1.1.30) (3-hydroxybutyrate dehydrogenase) (BDH)
Q99KR7	PPIF_MOUSE	Ppif	+	Ppif	Peptidyl-prolyl cis-trans isomerase F, mitochondrial (PPIase F) (EC 5.2.1.8) (Cyclophilin D) (CyP-D) (CypD) (Cyclophilin F) (Rotamase F)
Q9JLZ3	AUHM_MOUSE	Auh	+	Auh	Methylglutaconyl-CoA hydratase, mitochondrial (3-MG-CoA hydratase) (EC 4.2.1.18) (AU-specific RNA-binding enoyl-CoA hydratase) (AU-binding enoyl-CoA hydratase) (muAUH) (Itaconyl-CoA hydratase) (EC 4.2.1.56)
Q8QZT1	THIL_MOUSE	Acat1	+	Acat1	Acetyl-CoA acetyltransferase, mitochondrial (EC 2.3.1.9) (Acetoacetyl-CoA thiolase)
Q8CGK3	LONM_MOUSE	Lonp1	+	Lonp1 Prss15	Lon protease homolog, mitochondrial (EC 3.4.21.53) (Lon protease-like protein) (LONP) (Mitochondrial ATP-dependent protease Lon) (Serine protease 15)
Q9DCW4	ETFB_MOUSE	Etfb	+	Etfb	Electron transfer flavoprotein subunit beta (Beta-ETF)
Q9Z2I0	LETM1_MOUSE	Letm1	+	Letm1	Mitochondrial proton/calcium exchanger protein (Electroneutral mitochondrial K(+)/H(+)exchanger) (KHE) (Leucine zipper-EF-hand-containing transmembrane protein 1)
Q05920	PYC_MOUSE	Pc	+	Pc Pcx	Pyruvate carboxylase, mitochondrial (EC 6.4.1.1) (Pyruvic carboxylase) (PCB)
P38647	GRP75_MOUSE	Hspa9	+	Hspa9 Grp75 Hsp74 Hspa9a	Stress-70 protein, mitochondrial (75 kDa glucose-regulated protein) (GRP-75) (Heat shock 70 kDa protein 9) (Mortalin) (Peptide-binding protein 74) (PBP74) (p66 MOT)

Figure 5 shows the interaction of these 18 CLUH targets based on STRINGS database analysis. Reactome pathway analysis indicated proteins were related to respiratory election transport and ATP synthesis (yellow), mitochondrial import (pink), citric acid cycle (green), branched chain amino acid catabolism (purple) and utilization of ketone bodies (red).

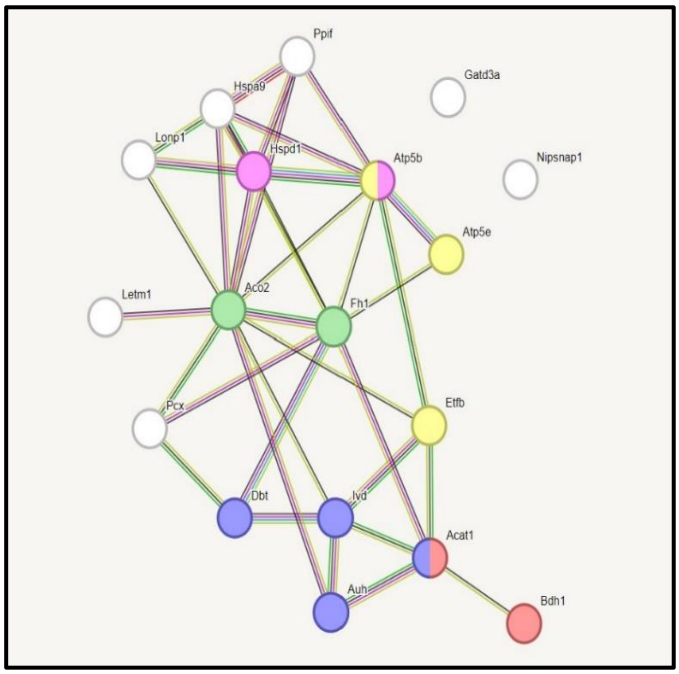

Figure 5. STRINGS pathway representation of the interaction of CLUH target proteins. Twenty-one enriched proteins were exclusively mitochondrially located. Of these, 18 were known CLUH targets. Reactome pathway analysis indicated proteins related to branched chain amino acid catabolism (purple), the citric acid cycle (green), respiratory election transport and ATP synthesis (yellow), the utilization of ketone bodies (red) and mitochondrial import (pink).

The strength and false discovery rate of the identified CLUH targets following Reactome pathway analysis are shown in Table 3.

Table 3. The strength and false discovery rate of the CLUH target proteins based on the Reactome pathway analysis.

Pathway	Description	Strength	False discovery rate	Colour code
MMU-70895	Branched-chain amino acid catabolism	2.39	5.68e-06	
MMU-71403	Citric acid cycle (TCA cycle)	2.04	0.0245	
MMU-163200	Respiratory electron transport, ATP synthesis by chemosmotic coupling and heat production by uncoupling proteins	1.49	0.0203	
MMU-77108	Utilization of Ketone Bodies	2.69	0.0056	
MMU-1268020	Mitochondrial protein import	2.43	0.0098	

SG formation is initiated by the activation of eIF2α via its phosphorylation by either PERK, HRI, GCN2 or PKR kinases (Taniuchi et al., 2016). GO analysis of the 134 enriched targets identified numerous

proteins involved in the pathways activating these four eIF2α-regulating kinases, as well as formation of SG-eIF2α complexes (Table 4).

Table 4. Proteins involved in the activation of the kinases known to form SGs.

Kinase	Pathway	GO terms	Strength	FDR	Description	Proteins
PERK	Unfolded proteins	GO:0000502	1.09	0.0049	Proteasome complex	Psmd1, Psmd7, Psmc3, Ecpas, Vcp
		GO:0030162	0.53	0.0028	regulation of proteolysis	Pebp1, Vcp, Psmc3, Park7, Hspd1, Prdx5
		GO:0005832	1.69	0.0034	chaperonin-containing T-	Cct2, Cct3, Cct7
		GO:0006914	0.71	0.0101	Autophagy	Vcp, Park7, Sqstm1, Map1lc3a, Clu, Pip4k2a, Sirt2, Cisd2, Arsb
		GO:0035966	0.87	0.0182	response to topologically incorrect protein	Vcp, Hspd1, Hspa9, Eifs1, Clu, Upf2
HRI	Oxidative stress	GO:0034599	0.8	0.0029	cellular response to oxidative stress	Sirt2, Cfl1, Prdx5, Park7, Ppif, Map1lc3a, Lonp1, Eif2s1, Pycr2
		GO:0000302	0.93	0.00014	response to reactive oxygen species	Cfl1, Prdx5, Park7, Prdx6, Hspd1, Ppif, Cryab, Kpna4, Gstp1, Map1lc3a
GCN2	Amino acid starvation	GO:0009083	1.59	0.00015	branched-chain amino acid catabolic process	Auh, Acat1, Ivd, Dbt, Bcat1
		GO:1901605	0.89	0.00083	alpha-amino acid metabolic process	Gclc, Bcat1, Mtap, Ass1, Pycr2, Psat1, Acat1, Ivd, Auh
		GO:0031667	0.56	0.0151	response to nutrient levels	Gcn1, Eif2s1, Lars, Apoe, Sirt2, Acat1, Arsb, Map1lc3a, Gstp1, Gclc, Fam107a, Ass1
		GO:0061771	2.04	0.0271	response to caloric restriction	Sirt2, Apoe
		GO:0006091	0.75	0.00024	generation of precursor metabolites and energy	Acat1, Etfb, Cs, Aco2, Fh1, Atp5e, Atp5b, Eno1b, Tpi, Tkt, Aldoa, Adh5, Prps1
		GO:0006418	1.49	5.0×10^{-7}	tRNA aminoacylation for protein translation	Vars, Iars, Wars, Yars, Eprs, Qars, Sars, Lars
PKR	dsRNA	GO:0044788	1.27	0.0106	modulation by host of viral	Apoe, Cfl1, Psmc3, Pcx
		GO:0019074	2.21	0.0198	viral RNA genome packaging	Pcx, Ddx6
SG-Eif2α	Global translation	GO:0006412	0.74	0.0003	translation	Aimp1, Lars, Sars, Wars, Yars, Iars, Qars, Vars, Eprs, Eef1g, Eefb2, Eif2s1, (rps27l)
		GO:0000932	1.01	0.0026	P-body	Edc4, Cnot1, Cnot9, Ddx6, Psmc3, Sqstm1
		GO:2001234	0.72	0.017	negative regulation of apoptotic signaling pathway	Hyou1, Gclc, Gstp1, Qars, Clu, Ppif, Park7, Eno1b

Figure 6 presents a hypothetical mechanistic framework, developed from our results and other published literature, linking acute TDP-43 cytoplasmic aggregation and SG formation to mitochondrial damage, sustained eIF2α activation and chronic SG formation, to eventual CLUH granule recruitment and MN and NMJ deterioration.

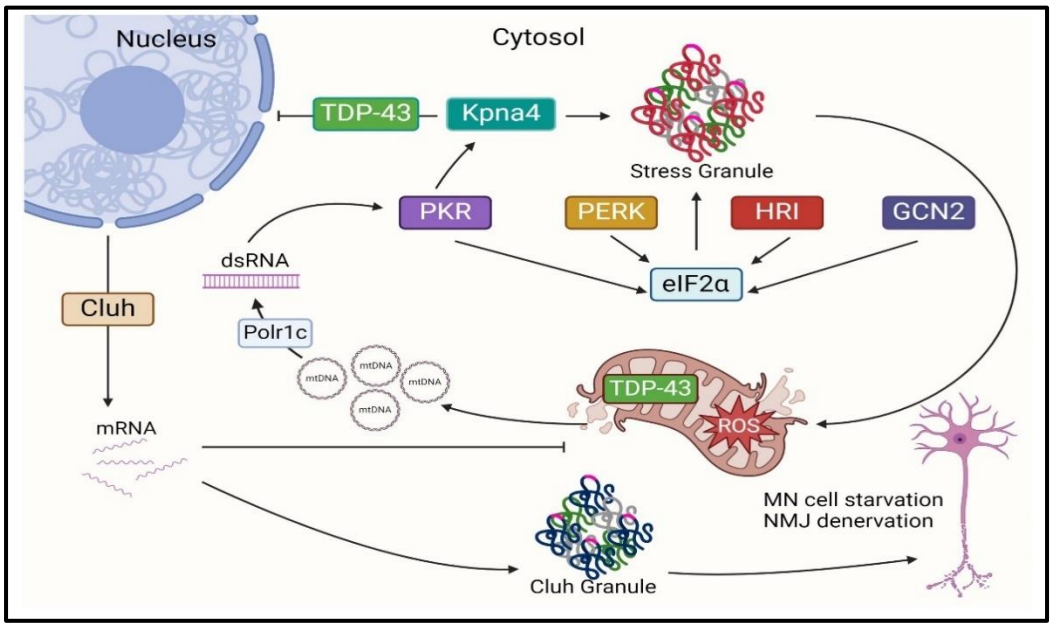

Figure 6. Theoretical model depicting the relationship between cytoplasmic TDP-43 and aggregation, SG formation, mitochondrial impairment and eventual NMJ and MN damage. TDP-43 accumulation and aggregation activate SG formation via multiple kinases upstream (PKR, PERK, HRI and GCN2) of eIF2α. The accumulative activation of these multiple kinase pathways and sustained SG formation would increase disease progression and severity due to persistent mitochondrial damage and mitochondrial DNA release into the cytoplasm, forming an escalating SG response. From the initial activation of the unfolded protein response via PERK, eIF2α phosphorylation activates the integrated stress response. This would cause a global halt to translation and suppression of apoptosis as the cells attempt to adapt to the stress. This recruits KPNA4 (Importin α3) into SGs, leading to the cytoplasmic accumulation of TDP-43. TDP-43 mitochondrial import would occur as a potential mechanism to remove excess TDP-43 via the ATP-dependent degradative action of LonP1, or to regulate mitochondrial metabolism. Excess mitochondrial TDP-43 would contribute to mitochondrial dysfunction, accumulation of ROS and activation of the HRI SG pathway. Prolonged cellular stress and eventual metabolic inflexibility would sequester CLUH (and its target mRNA/proteins) to the SG fraction to attenuate cellular anabolism. This would block mitophagy via loss of the CLUH target nipsnap1, causing damaged mitochondria to accumulate, followed by cytoplasmic mitochondrial DNA accumulation via the mPTP, as well as NMJ denervation and MN cell starvation. The cytoplasmic DNA is converted to RNA by Polr1c, which activates PKR and escalating the SG response. Created with Biorender.com.

We searched the literature to assist with placing our novel results in context of the human ALS condition. Recent work by Guise *et al* (Guise et al., 2024) performed single-cell proteomic profiling of postmortem ALS and control spinal cord MNs. They identified in the soluble fraction a depletion of several pathways in the ALS MNs, including SG formation, oxidative phosphorylation, BCAA degradation and the dynactin retrograde motor proteins. This was of interest as these pathways were enriched in our insoluble SG fraction from end-stage NEFH-TDP-43 brain tissue. We accessed the raw dataset from Guise *et al* (Guise et al., 2024) to compare the findings from both studies. A total of 540 proteins were selected from Supplemental Table 6 from the Guise *et al* dataset that were consistently depleted in ALS, when compared to control MNs (Guise et al., 2024) ($P<0.05$; Fold changes > 1.5), (Supplemental Table 4). These depleted proteins were entered into STRINGS and GO terms identified. We observed that 70% of the 540 depleted proteins from the soluble protein fraction from ALS MNs could be categorised into the five GO terms identified by the 134 enriched proteins from our insoluble SG protein fraction from brain tissue, including RNA binding (GO:0003723), ATP binding (GO:0005524), ribose phosphate metabolic process (GO:0019693), cellular component mitochondrion (GO:0005739) and cytoskeleton (GO:0005856) (Supplemental Table 4). Furthermore, there were 35 identified proteins common to both datasets (Table 5). Of the 540 depleted proteins, 67 were identified as known CLUH target proteins as shown on the STRINGS diagram in Figure 7.

Table 5. A list of the 35 proteins enriched in the insoluble SG fraction from end-stage NEFH-TDP-43 brain and depleted in the soluble protein fraction from ALS patients MNs.

Gene Names (primary)	Accession Mouse	Entry Name Mouse	Accession Human	Entry Name Humar	Gene Names	Protein names
ACOT7	Q91V12	BACH_MOUSE	O00154	BACH_HUMAN	Acot7 Bach	Cytosolic acyl coenzyme A thioester hydrolase (EC 3.1.2.2) (Acyl-CoA thioesterase 7) (Brain acyl-CoA hydrolase) (BACH) (CTE-IIa) (CTE-II) (Long chain acyl-CoA thioester hydrolase)
AIMP1	P31230	AIMP1_MOUSE	Q12904	AIMP1_HUMAN	Aimp1 Emap2 Scy	Aminoacyl tRNA synthase complex-interacting multifunctional protein 1 (Multisynthase complex auxiliary component p43) [Cleaved into: Endothelial monocyte-activating polypeptide 2 (EMAP-2) (Endothelial monocyte-activating polypeptide II) (EMAP-II) (Small inducible cytokine subfamily E member 1)]
ARHGDIA	Q99PT1	GDIR1_MOUSE	P52565	GDIR1_HUMAN	Arhgdia C87222 G	Rho GDP-dissociation inhibitor 1 (Rho GDI 1) (GDI-1) (Rho-GDI alpha)
ATP5F1B	P56480	ATPB_MOUSE	P06576	ATPB_HUMAN	Atp5f1b Atp5b	ATP synthase subunit beta, mitochondrial (EC 7.1.2.2) (ATP synthase F1 subunit beta)
AUH	Q9JLZ3	AUHM_MOUSE	Q13825	AUHM_HUMAN	Auh	Methylglutaconyl-CoA hydratase, mitochondrial (3-MG-CoA hydratase) (EC 4.2.1.18) (AU-specific RNA-binding enoyl-CoA hydratase) (AU-binding enoyl-CoA hydratase) (muAUH) (Itaconyl-CoA hydratase) (EC 4.2.1.56)
CCT2	P80314	TCPB_MOUSE	P78371	TCPB_HUMAN	Cct2 Cctb	T-complex protein 1 subunit beta (TCP-1-beta) (CCT-beta)
CCT3	P80318	TCPG_MOUSE	P49368	TCPG_HUMAN	Cct3 Cctg	T-complex protein 1 subunit gamma (TCP-1-gamma) (CCT-gamma) (Matricin) (mTRiC-P5)
CCT7	P80313	TCPH_MOUSE	Q99832	TCPH_HUMAN	Cct7 Ccth	T-complex protein 1 subunit eta (TCP-1-eta) (CCT-eta)
CLUH	Q5SW19	CLU_MOUSE	O75153	CLU_HUMAN	Cluh Kiaa0664	Clustered mitochondria protein homolog
CRMP1	P97427	DPYL1_MOUSE	Q14194	DPYL1_HUMAN	Crmp1 Dpysl1 Ulip	Dihydropyrimidinase-related protein 1 (DRP-1) (Collapsin response mediator protein 1) (CRMP-1) (Inactive dihydropyrimidinase) (Unc-33-like phosphoprotein 3) (ULIP-3)
DCTN1	O08788	DCTN1_MOUSE	Q14203	DCTN1_HUMAN	Dctn1	Dynactin subunit 1 (150 kDa dynein-associated polypeptide) (DAP-150) (DP-150) (p150-glued)
ECPAS	Q6PDI5	ECM29_MOUSE	Q5VYK3	ECM29_HUMAN	Ecpas Ecm29 Kiaa	Proteasome adapter and scaffold protein ECM29 (Proteasome-associated protein ECM29 homolog)
EEF1G	Q9D8N0	EF1G_MOUSE	P26641	EF1G_HUMAN	Eef1g	Elongation factor 1-gamma (EF-1-gamma) (eEF-1B gamma)
EPRS1	Q8CGC7	SYEP_MOUSE	P07814	SYEP_HUMAN	Eprs1 Eprs Qprs	Bifunctional glutamate/proline--tRNA ligase (Bifunctional aminoacyl-tRNA synthetase) [Includes: Glutamate--tRNA ligase (EC 6.1.1.17) (Glutamyl-tRNA synthetase) (GluRS); Proline--tRNA ligase (EC 6.1.1.15) (Prolyl-tRNA synthetase) (ProRS)]
FH	P97807	FUMH_MOUSE	P07954	FUMH_HUMAN	Fh Fh1	Fumarate hydratase, mitochondrial (Fumarase) (EC 4.2.1.2) (EF-3)
GSTO1	O09131	GSTO1_MOUSE	P78417	GSTO1_HUMAN	Gsto1 Gstx Gtsttl	Glutathione S-transferase omega-1 (GSTO-1) (EC 2.5.1.18) (Glutathione S-transferase omega 1-1) (GSTO 1-1) (Glutathione-dependent dehydroascorbate reductase) (EC 1.8.5.1) (Monomethylarsonic acid reductase) (MMA(V) reductase) (EC 1.20.4.2) (S-(Phenacyl)glutathione reductase) (SPG-R) (p28)
HINT1	P70349	HINT1_MOUSE	P49773	HINT1_HUMAN	Hint1 Hint Pkci Pk	Adenosine 5'-monophosphoramidase HINT1 (EC 3.9.1.-) (Desumoylating isopeptidase HINT1) (EC 3.4.22.-) (Histidine triad nucleotide-binding protein 1) (Protein kinase C inhibitor 1) (Protein kinase C-interacting protein 1) (PKCI-1)
HSPA9	P38647	GRP75_MOUSE	P38646	GRP75_HUMAN	Hspa9 Grp75 Hsp7	Stress-70 protein, mitochondrial (75 kDa glucose-regulated protein) (GRP-75) (Heat shock 70 kDa protein 9) (Mortalin) (Peptide-binding protein 74) (PBP74) (p66 MOT)
HSPD1	P63038	CH60_MOUSE	P10809	CH60_HUMAN	Hspd1 Hsp60	60 kDa heat shock protein, mitochondrial (EC 5.6.1.7) (60 kDa chaperonin) (Chaperonin 60) (CPN60) (HSP-65) (Heat shock protein 60) (HSP-60) (Hsp60) (Mitochondrial matrix protein P1)
HYOU1	Q9JKR6	HYOU1_MOUSE	Q9Y4L1	HYOU1_HUMAN	Hyou1 Grp170	Hypoxia up-regulated protein 1 (GRP-170) (140 kDa Ca(2+)-binding protein) (CBP-140)
IARS1	Q8BU30	SYIC_MOUSE	P41252	SYIC_HUMAN	Iars1 Iars	Isoleucine--tRNA ligase, cytoplasmic (EC 6.1.1.5) (Isoleucyl-tRNA synthetase) (IRS) (IleRS)
KPNA4	O35343	IMA3_MOUSE	O00629	IMA3_HUMAN	Kpna4 Qip1	Importin subunit alpha-3 (Importin alpha Q1) (Qip1) (Karyopherin subunit alpha-4)
LARS1	Q8BMJ2	SYLC_MOUSE	Q9P2J5	SYLC_HUMAN	Lars1 Lars	Leucine--tRNA ligase, cytoplasmic (EC 6.1.1.4) (Leucyl-tRNA synthetase) (LeuRS)
LETM1	Q9Z2I0	LETM1_MOUSE	O95202	LETM1_HUMAN	Letm1	Mitochondrial proton/calcium exchanger protein (Electroneutral mitochondrial K(+)/H(+)exchanger) (KHE) (Leucine zipper-EF-hand-containing transmembrane protein 1)
NIPSNAP1	O55125	NIPS1_MOUSE	Q9BPW8	NIPS1_HUMAN	Nipsnap1	Protein NipSnap homolog 1 (NipSnap1)
PC	Q05920	PYC_MOUSE	P11498	PYC_HUMAN	Pc Pcx	Pyruvate carboxylase, mitochondrial (EC 6.4.1.1) (Pyruvic carboxylase) (PCB)
PSMC3	O88685	PRS6A_MOUSE	P17980	PRS6A_HUMAN	Psmc3 Tbp1	26S proteasome regulatory subunit 6A (26S proteasome AAA-ATPase subunit RPT5) (Proteasome 26S subunit ATPase 3) (Tat-binding protein 1) (TBP-1)
PSMD1	Q3TXS7	PSMD1_MOUSE	Q99460	PSMD1_HUMAN	Psmd1	26S proteasome non-ATPase regulatory subunit 1 (26S proteasome regulatory subunit RPN2) (26S proteasome regulatory subunit S1)
PSMD7	P26516	PSMD7_MOUSE	P51665	PSMD7_HUMAN	Psmd7 Mov-34 Mc	26S proteasome non-ATPase regulatory subunit 7 (26S proteasome regulatory subunit RPN8) (26S proteasome regulatory subunit S12) (Mov34 protein) (Proteasome subunit p40)
QARS1	Q8BML9	SYQ_MOUSE	P47897	SYQ_HUMAN	Qars1 Qars	Glutamine--tRNA ligase (EC 6.1.1.18) (Glutaminyl-tRNA synthetase) (GlnRS)
SARS1	P26638	SYSC_MOUSE	P49591	SYSC_HUMAN	Sars1 Sars Sers	Serine--tRNA ligase, cytoplasmic (EC 6.1.1.11) (Seryl-tRNA synthetase) (SerRS) (Seryl-tRNA(Ser/Sec) synthetase)
TPI1	P17751	TPIS_MOUSE	P60174	TPIS_HUMAN	Tpi1 Tpi	Triosephosphate isomerase (TIM) (EC 5.3.1.1) (Methylglyoxal synthase) (EC 4.2.3.3) (Triose-phosphate isomerase)
UCHL1	Q9R0P9	UCHL1_MOUSE	P09936	UCHL1_HUMAN	Uchl1	Ubiquitin carboxyl-terminal hydrolase isozyme L1 (UCH-L1) (EC 3.4.19.12) (Neuron cytoplasmic protein 9.5) (PGP 9.5) (PGP9.5) (Ubiquitin thioesterase L1)
VARS1	Q9Z1Q9	SYVC_MOUSE	P26640	SYVC_HUMAN	Vars1 Bat6 G7a Va	Valine--tRNA ligase (EC 6.1.1.9) (Protein G7a) (Valyl-tRNA synthetase) (ValRS)
YARS1	Q91WQ3	SYYC_MOUSE	P54577	SYYC_HUMAN	Yars1 Yars	Tyrosine--tRNA ligase, cytoplasmic (EC 6.1.1.1) (Tyrosyl-tRNA synthetase) (TyrRS) [Cleaved into: Tyrosine--tRNA ligase, cytoplasmic, N-terminally processed]

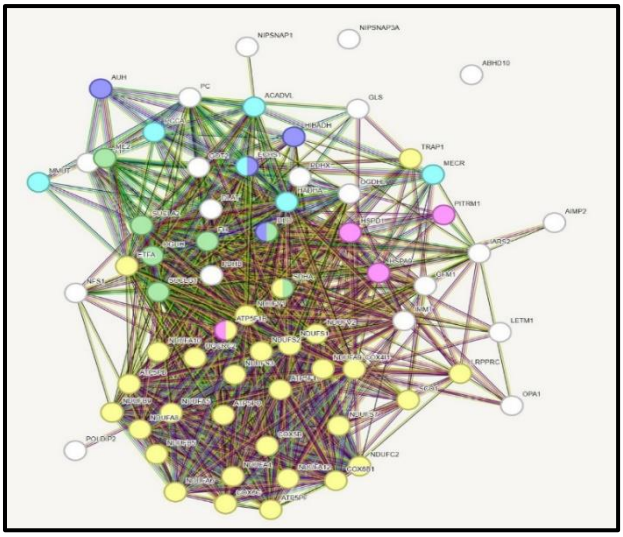

Figure 7. STRINGS pathway representation of the interaction between the 67 depleted CLUH proteins in the soluble protein fraction isolated from postmortem ALS and control MNs (Guise et al., 2024). These proteins were categorized into 5 GO terms including branched chain amino acid catabolism (purple), citric acid cycle (green), respiratory election transport and ATP synthesis (yellow), mitochondrial fatty-acid Beta-oxidation (blue) and mitochondrial import (pink).

The strength and false discovery rates for the Reactome pathway analysis are shown in Table 6. The descriptors and colour code relates to the proteins in Figure 7.

Table 6. The strength and false discovery rate of the depleted CLUH proteins from the soluble fraction from ALS MNs (Guise et al., 2024) based on the Reactome pathway analysis.

Pathway	Description	Strength	False discovery rate	Colour code
HAS-70895	Branched-chain amino acid catabolism	1.75	0.00018	
HSA-71403	Citric acid cycle (TCA cycle)	1.97	1.79e-09	
HSA-163200	Respiratory electron transport, ATP synthesis by chemosmotic coupling and heat production by uncoupling proteins	1.86	4.59e-45	
HSA-77289	Mitochondrial Beta-oxidation	1.68	1.27e-06	
HSA-1268020	Mitochondrial protein import	1.26	0.0075	

Having identified common proteins enriched in our insoluble SG fraction from brain tissue that were depleted in the soluble fraction of distal axons an additional dataset was also reanalysed. The depleted proteomics dataset of 245 proteins from the soluble fraction isolated from sciatic nerve of NEFH-TDP-43 mice from Altman *et al* (Altman et al., 2021) (Supplementary Table 5) was analysed by STRINGS. Of the five GO terms identified from our 134 enriched proteins from the insoluble TDP-43-associated brain SG fraction, the GO term Mitochondrion covered 55% of the depleted proteins identified in the soluble fraction of the NEFH-TDP-43 sciatic nerve preparation (135 of 245) by Altman *et al* (Altman et al., 2021). Other GO terms identified from the significantly depleted proteins in the Altman *et al*

dataset included BCAA, TCA and oxidative phosphorylation; GO terms also identified from the proteins enriched in our insoluble SG fraction from brain tissue.

Of the 245 proteins depleted in the Altman *et al* dataset 79 are known CLUH targets and are shown in the STRINGS diagram in Figure 8.

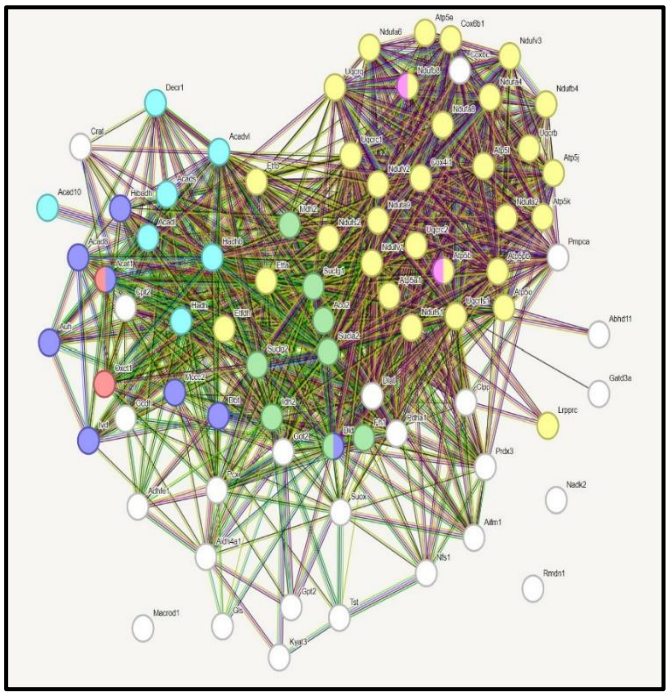

Figure 8. STRINGS pathway representation of the interaction between the 79 proteins depleted CLUH proteins in the soluble protein fraction sciatic nerve from the NEFH-TDP-43 mice (Altman et al., 2021). The 79 known CLUH targets were categorized into 6 GO terms including branched chain amino acid catabolism (purple), citric acid cycle (green), respiratory election transport and ATP synthesis (yellow), utilization of ketone bodies (red), mitochondrial protein import (pink), and mitochondrial fatty-acid Beta-oxidation (blue) oxidation (blue).

The strength and false discovery rates for the Reactome pathway analysis are shown in Table 7. The descriptors and colour code relates to the proteins in Figure 8.

Table 7. The strength and false discovery rate of the depleted CLUH proteins from the soluble fraction isolated from sciatic nerve of NEFH-TDP-43 mice (Altman *et al* 2021) based on the Reactome pathway analysis.

Pathway	Description	Strength	False discovery rate	Colour code
MMU-70895	Branched-chain amino acid catabolism	2.04	8.85e-12	
MMU-71403	Citric acid cycle (TCA cycle)	2.00	1.52e-11	
MMU-163200	Respiratory electron transport, ATP synthesis by chemosmotic coupling and heat production by uncoupling proteins	1.86	1.08e-44	
MMU-77108	Utilization of Ketone Bodies	2.04	0.0160	
MMU-1268020	Mitochondrial protein import	1.79	0.0341	
MMU-77289	Mitochondrial Fatty acid Beta-oxidation	1.72	2.68e-08	

Our analysis observed consistent overlap between proteins enriched in our insoluble TDP-43-associated brain SG fraction, that were also depleted in the soluble human ALS spinal MN fraction and soluble mouse sciatic nerve fractions. A Venn diagram showing the number of proteins commonly regulated in the three models is shown in Figure 9. When comparing the three datasets, 56 depleted targets are common between the soluble fractions from human spinal MNs and mouse sciatic nerve. Additionally, 35 proteins are common between our insoluble TDP-43-associated brain SG fraction (enriched) and the soluble human spinal MN fraction (depleted). There were four targets (PC, FH, AUH and ATP5F1B) common to all 3 datasets. Interestingly, these four are known CLUH targets.

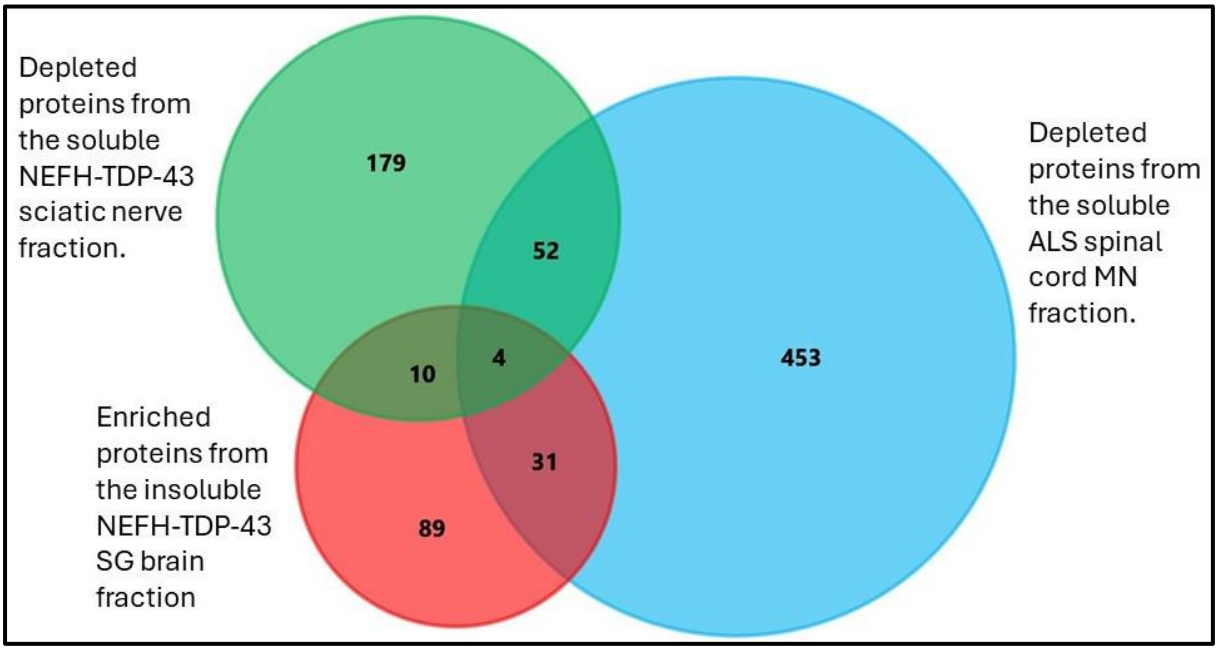

Figure 9. A Venn diagram showing the number of proteins that are enriched our insoluble TDP-43-associated brain SG fraction and also depleted in soluble human ALS spinal MN fraction (Guise et al. 2023) and soluble mouse sciatic nerve fraction (Altman et al. 2021).

Common overlap was also observed between the pathways regulated by CLUH and its target proteins. The common CLUH-regulated pathways enriched in our insoluble TDP-43-associated brain SG fraction, that were also depleted in soluble human ALS spinal MN fraction and soluble mouse sciatic nerve fractions are shown in Figure 10. These pathways were involved in BCCA catabolism, the citric acid cycle, respiratory electron transport/ATP synthesis and mitochondrial protein import. A table of all CLUH targets identified across all three datasets are shown in Supplementary Table 6.

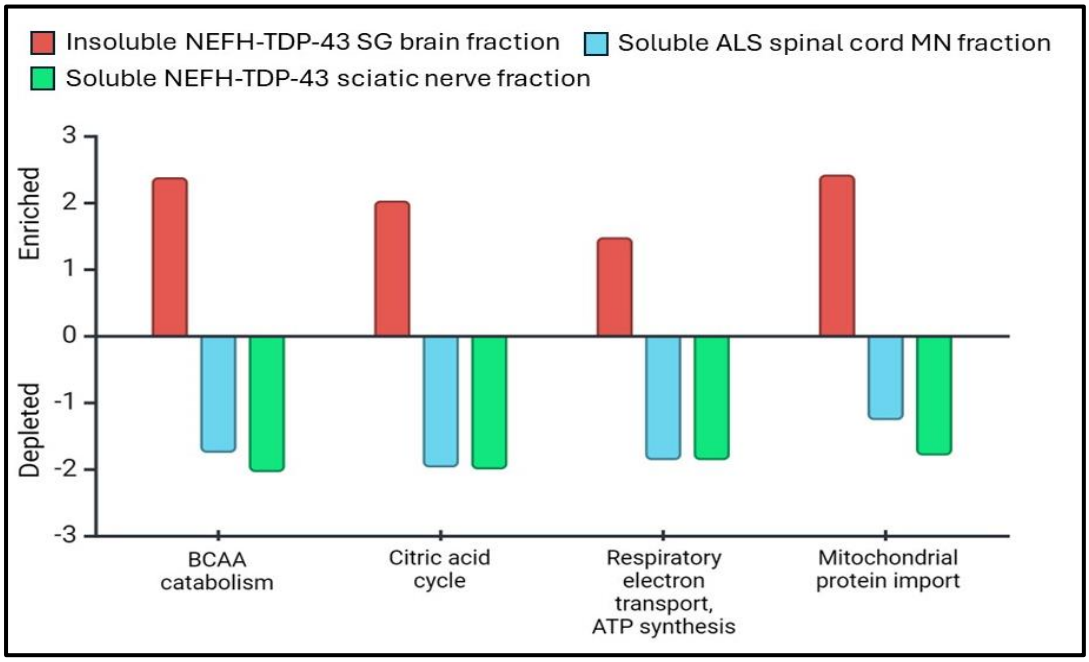

Figure 10. The strength and direction of the CLUH-regulated pathways identified from the proteins enriched in the insoluble TDP-43-associated brain SG fraction and depleted in soluble human ALS spinal MN fraction (Guise et al. 2023) and soluble mouse sciatic nerve fraction (Altman et al. 2021). Created with Biorender.com.

Discussion

The aim of the work was to isolate the insoluble TDP-43 associated SGs from the brain tissue of end stage NEFH-TDP-43 mice for subsequent proteomics analysis. Almost 5000 proteins were quantified from the cross-linked SG preparations from the TDP-43 mice. Approximately half of these proteins (2512) were SG and RNA binding proteins (RBPs). This was based on comparison with the comprehensive cell culture-derived Luenfield SG database consisting of 5732 proteins (as of 25/1/2024) (Millar et al., 2023). Our *in vivo* SG dataset also contained 71% of the proteins identified by G3BP1 immunoprecipitation from formaldehyde cross-linked, sodium arsenite stressed Human U-S

O2 cells (Jain et al., 2016). This supports the specificity of our modified formaldehyde cross-linking and TDP-43 (a core SG protein) immunoprecipitation protocol for use in tissue, that had previously been used in cultured cells (Jain et al., 2016). TDP-43-associated proteins have been previously analysed by proteomics from unstressed TDP-43 immunoprecipitated cell culture models (Evangelista et al., 2023; Freibaum et al., 2010; Vogler et al., 2018). However, analysis from different fractions (soluble and insoluble) makes comparisons challenging. It is also important to note that these variable sample preparations did not contain sample crosslinking (Evangelista et al., 2023; Freibaum et al., 2010; Vogler et al., 2018). We and others (Jain et al., 2016) have shown that sample crosslinking is essential for maintaining SG interactions during the stringent washing steps. Therefore, these cell culture-derived fractions are unlikely to contain significant SG aggregates. To the best of our knowledge, this is the first time an insoluble crosslinked TDP-43-associated SG fraction has been isolated from brain tissue of an ALS mouse model and its proteome reported.

The data presented here provides an end-stage snapshot of insoluble cytoplasmic TDP-43-associated SGs and other RBP partners. Analysis of the enriched proteins and an understanding of their respective pathways, and possible interactions, will shed light on potential ALS disease modifying mechanisms. From the ~5000 proteins quantified, a subset of 134 proteins were enriched and 17 proteins depleted, in the end-stage TDP-43 mouse brain tissue, compared with the control mice. Of these enriched proteins, 41 proteins were SG markers (Hu et al., 2023; Jain et al., 2016). Approximately 70% of the enriched dataset was covered by functional GO terms relating to binding of ATP and RNA, in addition to the biological processes, ribose phosphate metabolic process, and the cellular component's, cytoskeleton and mitochondrion. This is consistent with the idea that SGs are dynamic, ATP-dependent regulators of cellular metabolism (Jain et al., 2016; Wang et al., 2022). An unexpected and novel finding was the enrichment of the RNA binding protein CLUH, and a group of 17 CLUH targets (Gao et al., 2014; Schatton et al., 2017). To the best of our knowledge, CLUH regulation has not been highlighted previously in the ALS field. However, the presence of CLUH in our end-stage SG preparation may have considerable relevance for ALS pathogenesis, specifically in relation to mitochondrial function, MN and NMJ degeneration and metabolic flexibility. CLUH is the mRNA binding protein responsible for mitochondrial transport of nuclear encoded mitochondrial mRNA (Gao et al., 2014; Schatton et al., 2017; Wakim et al., 2017). CLUH is also required for neuronal development and motor neurone integrity (Zaninello et al., 2023). In response to glucose and amino acid starvation-induced stress, CLUH and its bound mRNAs form large RNP granules (Pla-Martin et al., 2020; Yang et al., 2022). These CLUH granules are formed as a survival mechanism to protect mRNAs from degradation and attenuate cellular anabolism (Pla-Martin et al., 2020; Yang et al., 2022). The loss of CLUH function

alters the mitochondrial proteome, impairs mitochondrial morphology and respiration, and elevates ROS production (Gao et al, 2014, Cox, Spradling 2009; Schatton Pla-Martoin, 2017; Sen, Cox, 2022; Wakim et al., 2017). Cultured liver cells from CLUH KO mice are highly glucose dependent and fail to shift from glucose to fat metabolism under starvation conditions (Schatton et al., 2017; Wakim et al., 2017). This highlights a role of CLUH in maintaining metabolic flexibility.

The CLUH targets identified in the TDP-43-associated SG fraction were enriched for the catabolic enzymes Acat1, Bcat1, Auh, Dbt, Ivd and Bdh1. These enzymes belong to the branched chain amino acid and ketone body pathways (Hwang et al., 2022; Jiang et al., 2022; Neinast et al., 2019). This suggests recruitment of CLUH to the TDP-43-associated SG fraction is a metabolic response to starvation in the end-stage brain of the NEFH-TDP-43 mice. The brain is usually protected from starvation and utilises glucose as a substrate (Harris et al., 2012; Oyarzabal & Marin-Valencia, 2019). However, it can use branched chain amino acids and ketone bodies, specifically leucine and β-hydroxybutyrate respectively (Divakaruni et al., 2017; Jensen et al., 2020). Although speculative, CLUH recruitment into the TDP-43-associated SG fraction would diminish its physiological role and contribute to the excessive impairment in mitochondrial function, as well as axonal and NMJ degradation seen in ALS (Altman et al., 2021; Zaninello et al., 2023). Identifying the point during ALS disease progression when CLUH is recruited to TDP-43-associated granules will be important to understand mechanisms of disease progression and potentially provide an opportunity for therapeutic intervention.

Mitochondrial dysfunction and impaired ATP production is well established in ALS and a consequence of multiple cellular disturbances (Muyderman & Chen, 2014; Zhao et al., 2022). Disrupted oxidative phosphorylation activates the pentose phosphate pathway (PPP) to generate cytoplasmic ATP (Skinner et al., 2023). Cell starvation, as indicated by CLUH recruitment into TDP-43-associated granules, would attenuate the provision of glycolytic and PPP substrates required for ATP production. Under such conditions ribose salvaging from RNA is activated as a carbon source for ATP generation. Our SG protein dataset was enriched for ribose salvaging from RNA for cytoplasmic ATP generation (GO:0019693 Ribose phosphate metabolic process). Furthermore, enrichment of Prps1, Tkt and Aldoa in our SG fraction suggests an impact on the PPP. Considering the fundamental role of SG formation, these PPP enzymes would be recruited into SGs to protect the untranslated mRNA. We speculate that the SG response and the CLUH granule response would prevent SG resolution, as this is an ATP dependent process (Jain et al., 2016). The positive effect of uridine supplementation on translation in CLUH KO motoneurons, supports this notion (Zaninello et al., 2023). From a therapeutic perspective,

uridine can substitute for ribose in the PPP, potentially sparing the RNA (Skinner et al., 2023). Uridine prevents ATP loss and *in vitro* cell death in glucose starved neurones in a dose dependent manner (Choi et al., 2008). In the context of ALS, uridine treatment extends the survival of SOD1G93A ALS mice and attenuates body weight loss, also in a dose dependent manner (Amante et al., 2010). This supports the notion of neuronal starvation in ALS. Oral uridine is poorly absorbed. However, the uridine pro-drug triacetyluridine, which is used for the treatment of 5-FU toxicity, results in supraphysiological uridine levels and is well absorbed by the gastrointestinal tract (Garcia et al., 2005). Triacetyluridine may therefore have a neuroprotective affect in ALS-induced neuronal starvation.

eIF2α activation initiates SG formation; the former phosphorylated by either PERK, HRI, GCN2 or PKR depending on the stressor (Taniuchi et al., 2016). In the NEFH-TDP-43 mice, over-expression of cytoplasmic mutated hTDP-43 protein is expected to activate SG formation via the unfolded protein response (UPR) detection of ER stress-activation and subsequent activation of the PERK pathway (Walker et al., 2013). This is supported by the enrichment of GO terms related to unfolded proteins (See table 2). Mitochondrial import of TDP-43 increases mitochondrial ROS production (Wang et al., 2019). Therefore, it was not unexpected to see enrichment of proteins associated with oxidative stress and ROS. This is consistent with activation of SGs via the HRI pathway (Basu et al., 2017). In addition to CLUH recruitment, the enriched proteins were associated with GO terms for amino acid starvation and nutrient levels. This supports SG activation via the GCN2 pathway (Hinnebusch & Fink, 1983). Additionally, there was an enrichment of GCN1, a direct activator of GCN2 (Cambiaghi et al., 2014), which detects the collision of ribosomes that are stalled during translation when amino acids become deficient (Lokdarshi & von Arnim, 2022). We also observed the enrichment of eight members of the Multi Synthetase complex (MCS), which act as an amino acid sensor to provide individual amino acids during protein translation (Hyeon et al., 2019), further suggesting GCN2 activation. Another novel observation was the enrichment of Polr1c in the TDP-43-associated SG fraction. The role of Polr1c is usually in the nucleus, however it also functions as a cytoplasmic DNA sensor. It activates the PKR-SG pathway, typically in response to viral infection (Chiu et al., 2009; Kessler & Maraia, 2021; Matsumiya et al., 2023). In the NEFH-TDP-43 mouse model, we suggest that SG formation may occur in response to TDP-43 entry into the mitochondria (Altman et al., 2021) and subsequent mitochondrial DNA release into the cytoplasm through the mitochondrial Permeability Transition Pore (mPTP) (Yu et al., 2020). The enrichment of Cyclophilin D (PPIF), which is part of mPTP (Yu et al., 2020), in the TDP-43-associated SG fraction supports this. Cytoplasmic Polr1c could convert the mitochondrial DNA to dsRNA and therefore activate PRK. It was unexpected to see evidence of activation of all four of the

Eif2α stress granule activation pathways. This raises the possibility that severe ALS pathology could be explained in terms of stress-related feedback loops resulting in persistent and progressive SG and CLUH granule recruitment with mitochondrial disruption leading to neuronal starvation and ATP crisis (Figure 6). Observations made in the soluble ALS patient-derived MN dataset (Guise et al., 2024) also support this, including downregulation of reactome pathways and GO terms relating to cellular response to starvation, response of EIF2AK4 (GCN2) to amino acid deficiency, response to ER stress (PERK), as well as downregulation of both PKR (E2AK2) and KPNA4 and enzymes involved in branched chain amino acid catabolism.

The presence of KPNA4 (also known as Importin α3) in our insoluble SG fraction is also unexpected as it acts as the nuclear import receptor for TDP-43. The mutations introduced into the nuclear localisation sequence (NLS) of TDP-43 abolish binding to Importin α3 (Park et al., 2020). This points to a couple of possibilities, including a potential limitation of formaldehyde cross-linking. Formaldehyde requires direct contact between molecules for a bond to be formed. However, cross-linking can also occur between molecules within a complex (Klockenbusch et al., 2012). This means that proteins enriched by immunoprecipitation with TDP-43 may not be in direct contact with TDP-43 but may be part of a complex with TDP-43. With this limitation in mind, the possibility that KPNA4 was recruited to the SG complex by another SG protein needs to be considered. For this to be mechanistically important, it would need to be early in the SG formation pathway. Indeed, KPNA4 can interact with PKR and eIF2α (Piazzi et al., 2019), the latter enriched in our SG dataset and a central regulator of SG formation (Kedersha et al., 2005). Recruitment of KPNA4 into the SG fraction from the transgenic NEFH-TDP-43 mice is most likely independent of TDP-43 due to its mutated NLS within the induced human TDP-43 protein. This observation is important and suggests a possible mechanism for TDP-43 cytoplasmic accumulation under pathophysiological ALS conditions. Cytoplasmic accumulation of TDP-43 is considered a hall mark of ALS and the mechanism by which this occurs remains unknown. However, there is evidence that disruption of the interaction of TDP-43 with its import receptors is a key part of this mechanism and SGs appear to be an integral part of this process (Prpar Mihevc et al., 2017; Zhang et al., 2018). In fact, in familial C9orf72 ALS, PKR is activated by RNA products from the random insertions in the C9orf72 gene (Parameswaran et al., 2023). This phosphorylates eIf2α and recruits Importin α3 (KPNA4) into SGs, resulting in TDP-43 cytoplasmic accumulation (Khosravi et al., 2017). Additionally, PKR inhibitors prevent eIf2α phosphorylation in C9orf72 and attenuate disease progression (Zu et al., 2020). As such, the PKR inhibitor Metformin, in addition to being used for the treatment of type II diabetes, is currently in clinical trial for fALS C9orf72 (Zu et al., 2020).

Analysis of the proteins depleted from the TDP-43-associated SG fraction identified several proteins with complimentary functions to the enriched protein data set, strengthening our interpretations. These depleted proteins included Dclk1, Zc3h3, PPP3CA and CLYD. Dclk1 is a kinase involved in the enhancement and inhibition of anterograde and retrograde transport, respectively in axons (Nawabi et al., 2015). Zc3h3 is a zinc finger protein required for nuclear export of mRNA and regulation of mRNA decay (Silla et al., 2020). Of significant interest, and in alignment with the enrichment of the CLUH-related granules, was the depletion of the calmodulin-dependent calcineurin A phosphatase (PPP3CA). PPP3CA dephosphorylates DNM1L (DRP1 was detected, but not enriched in our data set) in response to increased Ca2+ from mitochondrial depolarization (Cereghetti et al., 2008). Dephosphorylated Drp1 translocates from the cytoplasm to the mitochondria, via a CLUH-dependent mechanism (Yang et al., 2022). Here it triggers mitochondrial fission to separate damaged mitochondria, potentially in preparation for mitophagy (Yang et al., 2022; Zerihun et al., 2023). There was depletion in the Ubiquitin carboxyl-terminal hydrolase (CLYD) protein. CLYD promotes microtubule stabilisation by inhibiting HDAC6 deacetylation of alpha-tubulin (Wickstrom et al., 2010). Interestingly, there was enrichment for Tubulin deacetylation (GO:0090042), including the Tubulin deacetylase, Sirt1. Combined, these observations are consistent with the importance of tubulin acetylation in axonal transport in ALS (Guo et al., 2017).

Analysis of the soluble ALS patient-derived MN dataset (Guise et al., 2024) and comparison with our results, sheds some light on how TDP-43 associated SGs may have a broad impact on multiple cellular pathways. Several functional networks enriched in our insoluble TDP-43 associated SGs brain dataset were downregulated in the soluble spinal cord MN dataset (Guise et al., 2024), including proteasome complex, chaperonin-containing T-complex, tRNA aminoacylation for protein translation, TCA and oxidative phosphorylation. These inverse changes in the functional networks from insoluble brain and soluble MN samples is consistent with the role of RBPs and RNA granules in the transport of mRNA for local translation in distal axons of MNs (Altman et al., 2021; Piol et al., 2023). For example, CLUH has a specific role in the transport and stability of nuclear encoded mitochondrial mRNA in MNs and maintenance of the NMJ (Zaninello et al., 2023). The recruitment of CLUH and CLUH target mRNA to the insoluble TDP-43-associated SG fraction in the brain may result in depletion of these same molecules in the functional soluble component in distal axons of MNs. Indeed, observations made *ex vivo,* that CLUH and 64 CLUH target proteins were depleted in the soluble fraction of ALS patient MNs is striking (Guise et al., 2024). Importantly, five of the depleted CLUH target proteins (Gao et al., 2014; Schatton et al., 2017) were also our enriched dataset (Nipsnap1, Hspd1, Atp5f1b, Letm1 and Pc). Reanalysis of the Altman *et al* dataset of depleted proteins in the soluble fraction from sciatic nerves

of the NEFH-TDP-43 mice, which is heavily skewed for mitochondrial proteins, revealed that 33% of the total depleted dataset are known CLUH targets. These two axon-derived depleted protein datasets support a link between the formation of insoluble SG aggregates and protein depletion in the soluble protein pool. Furthermore, the datasets highlight a likely role of CLUH in this depletion. STRINGS analysis identified retrograde dynactin motor components enriched in our insoluble SG dataset (Dcnt1, Dctn2, Actr1b and Actr10) and depleted in the soluble ALS patient MNs samples (Dctn1, Actr1a, Dync1li2, Dync1i1, Dynll1, Dync1h1, and Dync1li1). Additionally, imaging experiments of TDP-43-containing granules conducted in ALS patient iPSC-derived neurons, shows a specific increase in retrograde axonal transport (Alami et al., 2014). This suggests the mechanism of depletion of CLUH target proteins from MNs by TDP-43-associated granules is via enhanced retrograde transport.

Here we have observed that the insoluble TDP-43-associated SG proteome from end-stage NEFH-TDP-43 brain tissue is enriched with not only well-studied SG markers, but also enriched with numerous other proteins. Integration of these unexpected SG-bound proteins suggests activation of multiple SG forming pathways, mitochondrial damage and cytoplasmic presence of mitochondrial DNA; the later forming a loop for sustained SG formation. We have provided a hypothetical mechanistic framework, based on the interpretation of our results and in conjunction with published literature, demonstrating how alterations in the pathways may intersect to create a toxic environment resulting in MN and NMJ degeneration (Figure 6). The presence of CLUH is of significant interest considering its role in mitochondrial and neuronal homeostasis and should be considered as a novel target regulating ALS pathogenesis. Understanding the temporal formation and composition of this SG fraction will further identify key disease modifying proteins and pathways influencing ALS.

References

Advani, V. M., & Ivanov, P. (2019). Translational Control under Stress: Reshaping the Translatome. *Bioessays*, *41*(5), e1900009. https://doi.org/10.1002/bies.201900009

Alami, N. H., Smith, R. B., Carrasco, M. A., Williams, L. A., Winborn, C. S., Han, S. S. W., Kiskinis, E., Winborn, B., Freibaum, B. D., Kanagaraj, A., Clare, A. J., Badders, N. M., Bilican, B., Chaum, E., Chandran, S., Shaw, C. E., Eggan, K. C., Maniatis, T., & Taylor, J. P. (2014). Axonal transport of TDP-43 mRNA granules is impaired by ALS-causing mutations. *Neuron*, *81*(3), 536-543. https://doi.org/10.1016/j.neuron.2013.12.018

Altman, T., Ionescu, A., Ibraheem, A., Priesmann, D., Gradus-Pery, T., Farberov, L., Alexandra, G., Shelestovich, N., Dafinca, R., Shomron, N., Rage, F., Talbot, K., Ward, M. E., Dori, A., Kruger, M., & Perlson, E. (2021). Axonal TDP-43 condensates drive neuromuscular junction disruption through inhibition of local synthesis of nuclear encoded mitochondrial proteins. *Nat Commun*, *12*(1), 6914. https://doi.org/10.1038/s41467-021-27221-8

Arai, T., Hasegawa, M., Akiyama, H., Ikeda, K., Nonaka, T., Mori, H., Mann, D., Tsuchiya, K., Yoshida, M., Hashizume, Y., & Oda, T. (2006). TDP-43 is a component of ubiquitin-positive tau-negative inclusions in frontotemporal lobar degeneration and amyotrophic lateral sclerosis. *Biochem Biophys Res Commun*, *351*(3), 602-611. https://doi.org/10.1016/j.bbrc.2006.10.093

Asadi, M. R., Sadat Moslehian, M., Sabaie, H., Jalaiei, A., Ghafouri-Fard, S., Taheri, M., & Rezazadeh, M. (2021). Stress Granules and Neurodegenerative Disorders: A Scoping Review. *Front Aging Neurosci*, *13*, 650740. https://doi.org/10.3389/fnagi.2021.650740

Basu, M., Courtney, S. C., & Brinton, M. A. (2017). Arsenite-induced stress granule formation is inhibited by elevated levels of reduced glutathione in West Nile virus-infected cells. *PLoS Pathog*, *13*(2), e1006240. https://doi.org/10.1371/journal.ppat.1006240

Cambiaghi, T. D., Pereira, C. M., Shanmugam, R., Bolech, M., Wek, R. C., Sattlegger, E., & Castilho, B. A. (2014). Evolutionarily conserved IMPACT impairs various stress responses that require GCN1 for activating the eIF2 kinase GCN2. *Biochem Biophys Res Commun*, *443*(2), 592-597. https://doi.org/10.1016/j.bbrc.2013.12.021

Cereghetti, G. M., Stangherlin, A., Martins de Brito, O., Chang, C. R., Blackstone, C., Bernardi, P., & Scorrano, L. (2008). Dephosphorylation by calcineurin regulates translocation of Drp1 to mitochondria. *Proc Natl Acad Sci U S A*, *105*(41), 15803-15808. https://doi.org/10.1073/pnas.0808249105

Choi, J. W., Shin, C. Y., Choi, M. S., Yoon, S. Y., Ryu, J. H., Lee, J. C., Kim, W. K., El Kouni, M. H., & Ko, K. H. (2008). Uridine protects cortical neurons from glucose deprivation-induced death: possible role of uridine phosphorylase. *J Neurotrauma*, *25*(6), 695-707. https://doi.org/10.1089/neu.2007.0409

Colombrita, C., Zennaro, E., Fallini, C., Weber, M., Sommacal, A., Buratti, E., Silani, V., & Ratti, A. (2009). TDP-43 is recruited to stress granules in conditions of oxidative insult. *J Neurochem*, *111*(4), 1051-1061. https://doi.org/10.1111/j.1471-4159.2009.06383.x

Daigle, J. G., Krishnamurthy, K., Ramesh, N., Casci, I., Monaghan, J., McAvoy, K., Godfrey, E. W., Daniel, D. C., Johnson, E. M., Monahan, Z., Shewmaker, F., Pasinelli, P., & Pandey, U. B. (2016). Pur-alpha regulates cytoplasmic stress granule dynamics and ameliorates FUS toxicity. *Acta Neuropathol*, *131*(4), 605-620. https://doi.org/10.1007/s00401-015-1530-0

Divakaruni, A. S., Wallace, M., Buren, C., Martyniuk, K., Andreyev, A. Y., Li, E., Fields, J. A., Cordes, T., Reynolds, I. J., Bloodgood, B. L., Raymond, L. A., Metallo, C. M., & Murphy, A. N. (2017). Inhibition of the mitochondrial pyruvate carrier protects from excitotoxic neuronal death. *J Cell Biol*, *216*(4), 1091-1105. https://doi.org/10.1083/jcb.201612067

Evangelista, B. A., Cahalan, S. R., Ragusa, J. V., Mordant, A., Necarsulmer, J. C., Perna, R. J., Ajit, T., White, K., Barker, N. K., Tian, X., Cohen, S., Meeker, R., Herring, L. E., & Cohen, T. J. (2023). Tandem detergent-extraction and immunoprecipitation of proteinopathy: Scalable

enrichment of ALS-associated TDP-43 aggregates. *iScience*, *26*(5), 106645. https://doi.org/10.1016/j.isci.2023.106645

Fan, A. C., & Leung, A. K. (2016). RNA Granules and Diseases: A Case Study of Stress Granules in ALS and FTLD. *Adv Exp Med Biol*, *907*, 263-296. https://doi.org/10.1007/978-3-319-29073-7_11

Freibaum, B. D., Chitta, R. K., High, A. A., & Taylor, J. P. (2010). Global analysis of TDP-43 interacting proteins reveals strong association with RNA splicing and translation machinery. *Journal of proteome research*, *9*(2), 1104-1120.

Gao, J., Schatton, D., Martinelli, P., Hansen, H., Pla-Martin, D., Barth, E., Becker, C., Altmueller, J., Frommolt, P., Sardiello, M., & Rugarli, E. I. (2014). CLUH regulates mitochondrial biogenesis by binding mRNAs of nuclear-encoded mitochondrial proteins. *J Cell Biol*, *207*(2), 213-223. https://doi.org/10.1083/jcb.201403129

Guise, A. J., Misal, S. A., Carson, R., Chu, J. H., Boekweg, H., Van Der Watt, D., Welsh, N. C., Truong, T., Liang, Y., Xu, S., Benedetto, G., Gagnon, J., Payne, S. H., Plowey, E. D., & Kelly, R. T. (2024). TDP-43-stratified single-cell proteomics of postmortem human spinal motor neurons reveals protein dynamics in amyotrophic lateral sclerosis. *Cell Rep*, *43*(1), 113636. https://doi.org/10.1016/j.celrep.2023.113636

Guo, W., Naujock, M., Fumagalli, L., Vandoorne, T., Baatsen, P., Boon, R., Ordovas, L., Patel, A., Welters, M., Vanwelden, T., Geens, N., Tricot, T., Benoy, V., Steyaert, J., Lefebvre-Omar, C., Boesmans, W., Jarpe, M., Sterneckert, J., Wegner, F., . . . Van Den Bosch, L. (2017). HDAC6 inhibition reverses axonal transport defects in motor neurons derived from FUS-ALS patients. *Nat Commun*, *8*(1), 861. https://doi.org/10.1038/s41467-017-00911-y

Harris, J. J., Jolivet, R., & Attwell, D. (2012). Synaptic energy use and supply. *Neuron*, *75*(5), 762-777. https://doi.org/10.1016/j.neuron.2012.08.019

Hasegawa, M., Arai, T., Nonaka, T., Kametani, F., Yoshida, M., Hashizume, Y., Beach, T. G., Buratti, E., Baralle, F., Morita, M., Nakano, I., Oda, T., Tsuchiya, K., & Akiyama, H. (2008). Phosphorylated TDP-43 in frontotemporal lobar degeneration and amyotrophic lateral sclerosis. *Ann Neurol*, *64*(1), 60-70. https://doi.org/10.1002/ana.21425

Hergesheimer, R. C., Chami, A. A., de Assis, D. R., Vourc'h, P., Andres, C. R., Corcia, P., Lanznaster, D., & Blasco, H. (2019). The debated toxic role of aggregated TDP-43 in amyotrophic lateral sclerosis: a resolution in sight? *Brain*, *142*(5), 1176-1194. https://doi.org/10.1093/brain/awz078

Hinnebusch, A. G., & Fink, G. R. (1983). Positive regulation in the general amino acid control of Saccharomyces cerevisiae. *Proc Natl Acad Sci U S A*, *80*(17), 5374-5378. https://doi.org/10.1073/pnas.80.17.5374

Hu, S., Zhang, Y., Yi, Q., Yang, C., Liu, Y., & Bai, Y. (2023). Time-resolved proteomic profiling reveals compositional and functional transitions across the stress granule life cycle. *Nat Commun*, *14*(1), 7782. https://doi.org/10.1038/s41467-023-43470-1

Hughes, C. S., Moggridge, S., Muller, T., Sorensen, P. H., Morin, G. B., & Krijgsveld, J. (2019). Single-pot, solid-phase-enhanced sample preparation for proteomics experiments. *Nat Protoc*, *14*(1), 68-85. https://doi.org/10.1038/s41596-018-0082-x

Hwang, C. Y., Choe, W., Yoon, K. S., Ha, J., Kim, S. S., Yeo, E. J., & Kang, I. (2022). Molecular Mechanisms for Ketone Body Metabolism, Signaling Functions, and Therapeutic Potential in Cancer. *Nutrients*, *14*(22). https://doi.org/10.3390/nu14224932

Hyeon, D. Y., Kim, J. H., Ahn, T. J., Cho, Y., Hwang, D., & Kim, S. (2019). Evolution of the multi-tRNA synthetase complex and its role in cancer. *J Biol Chem*, *294*(14), 5340-5351. https://doi.org/10.1074/jbc.REV118.002958

Inukai, Y., Nonaka, T., Arai, T., Yoshida, M., Hashizume, Y., Beach, T. G., Buratti, E., Baralle, F. E., Akiyama, H., Hisanaga, S., & Hasegawa, M. (2008). Abnormal phosphorylation of Ser409/410 of TDP-43 in FTLD-U and ALS. *FEBS Lett*, *582*(19), 2899-2904. https://doi.org/10.1016/j.febslet.2008.07.027

Jain, S., Wheeler, J. R., Walters, R. W., Agrawal, A., Barsic, A., & Parker, R. (2016). ATPase-Modulated Stress Granules Contain a Diverse Proteome and Substructure. *Cell*, *164*(3), 487-498. https://doi.org/10.1016/j.cell.2015.12.038

Jensen, N. J., Wodschow, H. Z., Nilsson, M., & Rungby, J. (2020). Effects of Ketone Bodies on Brain Metabolism and Function in Neurodegenerative Diseases. *International journal of molecular sciences*, *21*(22). https://doi.org/10.3390/ijms21228767

Jiang, Z., Zheng, J., Liu, J., Yang, X., & Chen, K. (2022). Novel Branched-Chain Amino Acid-Catabolism Related Gene Signature for Overall Survival Prediction of Pancreatic Carcinoma. *J Proteome Res*, *21*(3), 740-746. https://doi.org/10.1021/acs.jproteome.1c00607

Kedersha, N., Cho, M. R., Li, W., Yacono, P. W., Chen, S., Gilks, N., Golan, D. E., & Anderson, P. (2000). Dynamic Shuttling of Tia-1 Accompanies the Recruitment of mRNA to Mammalian Stress Granules. *Journal of Cell Biology*, *151*(6), 1257-1268. https://doi.org/10.1083/jcb.151.6.1257

Kedersha, N., Stoecklin, G., Ayodele, M., Yacono, P., Lykke-Andersen, J., Fritzler, M. J., Scheuner, D., Kaufman, R. J., Golan, D. E., & Anderson, P. (2005). Stress granules and processing bodies are dynamically linked sites of mRNP remodeling. *J Cell Biol*, *169*(6), 871-884. https://doi.org/10.1083/jcb.200502088

Klockenbusch, C., O'Hara, J. E., & Kast, J. (2012). Advancing formaldehyde cross-linking towards quantitative proteomic applications. *Anal Bioanal Chem*, *404*(4), 1057-1067. https://doi.org/10.1007/s00216-012-6065-9

Lee, A., Henderson, R., Arachchige, B. J., Robertson, T., & McCombe, P. A. (2023). Proteomic investigation of ALS motor cortex identifies known and novel pathogenetic mechanisms. *J Neurol Sci*, *452*, 120753. https://doi.org/10.1016/j.jns.2023.120753

Lepine, S., Castellanos-Montiel, M. J., & Durcan, T. M. (2022). TDP-43 dysregulation and neuromuscular junction disruption in amyotrophic lateral sclerosis. *Transl Neurodegener*, *11*(1), 56. https://doi.org/10.1186/s40035-022-00331-z

Ling, S. C., Polymenidou, M., & Cleveland, D. W. (2013). Converging mechanisms in ALS and FTD: disrupted RNA and protein homeostasis. *Neuron*, *79*(3), 416-438. https://doi.org/10.1016/j.neuron.2013.07.033

Liu-Yesucevitz, L., Bilgutay, A., Zhang, Y. J., Vanderweyde, T., Citro, A., Mehta, T., Zaarur, N., McKee, A., Bowser, R., Sherman, M., Petrucelli, L., & Wolozin, B. (2010). Tar DNA binding protein-43 (TDP-43) associates with stress granules: analysis of cultured cells and pathological brain tissue. *PLoS One*, *5*(10), e13250. https://doi.org/10.1371/journal.pone.0013250

Lokdarshi, A., & von Arnim, A. G. (2022). Review: Emerging roles of the signaling network of the protein kinase GCN2 in the plant stress response. *Plant Sci*, *320*, 111280. https://doi.org/10.1016/j.plantsci.2022.111280

Matsumiya, T., Shiba, Y., Ding, J., Kawaguchi, S., Seya, K., & Imaizumi, T. (2023). The double-stranded RNA-dependent protein kinase PKR negatively regulates the protein expression of IFN-beta induced by RIG-I signaling. *Faseb j*, *37*(2), e22780. https://doi.org/10.1096/fj.202201520RR

McDonald, K. K., Aulas, A., Destroismaisons, L., Pickles, S., Beleac, E., Camu, W., Rouleau, G. A., & Vande Velde, C. (2011). TAR DNA-binding protein 43 (TDP-43) regulates stress granule dynamics via differential regulation of G3BP and TIA-1. *Hum Mol Genet*, *20*(7), 1400-1410. https://doi.org/10.1093/hmg/ddr021

Millar, S. R., Huang, J. Q., Schreiber, K. J., Tsai, Y. C., Won, J., Zhang, J., Moses, A. M., & Youn, J. Y. (2023). A New Phase of Networking: The Molecular Composition and Regulatory Dynamics of Mammalian Stress Granules. *Chem Rev*, *123*(14), 9036-9064. https://doi.org/10.1021/acs.chemrev.2c00608

Montalbano, M., McAllen, S., Cascio, F. L., Sengupta, U., Garcia, S., Bhatt, N., Ellsworth, A., Heidelman, E. A., Johnson, O. D., Doskocil, S., & Kayed, R. (2020). TDP-43 and Tau Oligomers in Alzheimer's Disease, Amyotrophic Lateral Sclerosis, and Frontotemporal Dementia. *Neurobiol Dis*, *146*, 105130. https://doi.org/10.1016/j.nbd.2020.105130

Morgenstern, M., Peikert, C. D., Lubbert, P., Suppanz, I., Klemm, C., Alka, O., Steiert, C., Naumenko, N., Schendzielorz, A., Melchionda, L., Muhlhauser, W. W. D., Knapp, B., Busch, J. D., Stiller, S. B., Dannenmaier, S., Lindau, C., Licheva, M., Eickhorst, C., Galbusera, R., . . . Warscheid, B. (2021). Quantitative high-confidence human mitochondrial proteome and its dynamics in cellular context. *Cell Metab*, *33*(12), 2464-2483 e2418. https://doi.org/10.1016/j.cmet.2021.11.001

Muyderman, H., & Chen, T. (2014). Mitochondrial dysfunction in amyotrophic lateral sclerosis - a valid pharmacological target? *Br J Pharmacol*, *171*(8), 2191-2205. https://doi.org/10.1111/bph.12476

Nawabi, H., Belin, S., Cartoni, R., Williams, P. R., Wang, C., Latremoliere, A., Wang, X., Zhu, J., Taub, D. G., Fu, X., Yu, B., Gu, X., Woolf, C. J., Liu, J. S., Gabel, C. V., Steen, J. A., & He, Z. (2015). Doublecortin-Like Kinases Promote Neuronal Survival and Induce Growth Cone Reformation via Distinct Mechanisms. *Neuron*, *88*(4), 704-719. https://doi.org/10.1016/j.neuron.2015.10.005

Neinast, M., Murashige, D., & Arany, Z. (2019). Branched Chain Amino Acids. *Annu Rev Physiol*, *81*, 139-164. https://doi.org/10.1146/annurev-physiol-020518-114455

Neumann, M., Sampathu, D. M., Kwong, L. K., Truax, A. C., Micsenyi, M. C., Chou, T. T., Bruce, J., Schuck, T., Grossman, M., Clark, C. M., McCluskey, L. F., Miller, B. L., Masliah, E., Mackenzie, I. R., Feldman, H., Feiden, W., Kretzschmar, H. A., Trojanowski, J. Q., & Lee, V. M. (2006). Ubiquitinated TDP-43 in frontotemporal lobar degeneration and amyotrophic lateral sclerosis. *Science*, *314*(5796), 130-133. https://doi.org/10.1126/science.1134108

Ohn, T., Kedersha, N., Hickman, T., Tisdale, S., & Anderson, P. (2008). A functional RNAi screen links O-GlcNAc modification of ribosomal proteins to stress granule and processing body assembly. *Nat Cell Biol*, *10*(10), 1224-1231. https://doi.org/10.1038/ncb1783

Oyarzabal, A., & Marin-Valencia, I. (2019). Synaptic energy metabolism and neuronal excitability, in sickness and health. *J Inherit Metab Dis*, *42*(2), 220-236. https://doi.org/10.1002/jimd.12071

Parameswaran, J., Zhang, N., Braems, E., Tilahun, K., Pant, D. C., Yin, K., Asress, S., Heeren, K., Banerjee, A., Davis, E., Schwartz, S. L., Conn, G. L., Bassell, G. J., Van Den Bosch, L., & Jiang, J. (2023). Antisense, but not sense, repeat expanded RNAs activate PKR/eIF2alpha-dependent ISR in C9ORF72 FTD/ALS. *Elife*, *12*. https://doi.org/10.7554/eLife.85902

Park, J. H., Chung, C. G., Park, S. S., Lee, D., Kim, K. M., Jeong, Y., Kim, E. S., Cho, J. H., Jeon, Y. M., Shen, C. J., Kim, H. J., Hwang, D., & Lee, S. B. (2020). Cytosolic calcium regulates cytoplasmic accumulation of TDP-43 through Calpain-A and Importin alpha3. *Elife*, *9*. https://doi.org/10.7554/eLife.60132

Piazzi, M., Bavelloni, A., Gallo, A., Faenza, I., & Blalock, W. L. (2019). Signal Transduction in Ribosome Biogenesis: A Recipe to Avoid Disaster. *International journal of molecular sciences*, *20*(11). https://doi.org/10.3390/ijms20112718

Piol, D., Robberechts, T., & Da Cruz, S. (2023). Lost in local translation: TDP-43 and FUS in axonal/neuromuscular junction maintenance and dysregulation in amyotrophic lateral sclerosis. *Neuron*, *111*(9), 1355-1380. https://doi.org/10.1016/j.neuron.2023.02.028

Prasad, A., Bharathi, V., Sivalingam, V., Girdhar, A., & Patel, B. K. (2019). Molecular Mechanisms of TDP-43 Misfolding and Pathology in Amyotrophic Lateral Sclerosis. *Front Mol Neurosci*, *12*, 25. https://doi.org/10.3389/fnmol.2019.00025

Prpar Mihevc, S., Darovic, S., Kovanda, A., Bajc Cesnik, A., Zupunski, V., & Rogelj, B. (2017). Nuclear trafficking in amyotrophic lateral sclerosis and frontotemporal lobar degeneration. *Brain*, *140*(1), 13-26. https://doi.org/10.1093/brain/aww197

San Gil, R., Pascovici, D., Venturato, J., Brown-Wright, H., Mehta, P., Madrid San Martin, L., Wu, J., Luan, W., Chui, Y. K., Bademosi, A. T., Swaminathan, S., Naidoo, S., Berning, B. A., Wright, A. L., Keating, S. S., Curtis, M. A., Faull, R. L. M., Lee, J. D., Ngo, S. T., . . . Walker, A. K. (2024). A transient protein folding response targets aggregation in the early phase of TDP-43-mediated neurodegeneration. *Nat Commun*, *15*(1), 1508. https://doi.org/10.1038/s41467-024-45646-9

Santamaria, N., Alhothali, M., Alfonso, M. H., Breydo, L., & Uversky, V. N. (2017). Intrinsic disorder in proteins involved in amyotrophic lateral sclerosis. *Cellular and molecular life sciences : CMLS*, *74*(7), 1297-1318. https://doi.org/10.1007/s00018-016-2416-6

Sap, K. A., Guler, A. T., Bury, A., Dekkers, D., Demmers, J. A. A., & Reits, E. A. (2021). Identification of Full-Length Wild-Type and Mutant Huntingtin Interacting Proteins by Crosslinking Immunoprecipitation in Mice Brain Cortex. *J Huntingtons Dis*, *10*(3), 335-347. https://doi.org/10.3233/JHD-210476

Schatton, D., Pla-Martin, D., Marx, M. C., Hansen, H., Mourier, A., Nemazanyy, I., Pessia, A., Zentis, P., Corona, T., Kondylis, V., Barth, E., Schauss, A. C., Velagapudi, V., & Rugarli, E. I. (2017). CLUH regulates mitochondrial metabolism by controlling translation and decay of target mRNAs. *J Cell Biol*, *216*(3), 675-693. https://doi.org/10.1083/jcb.201607019

Skinner, O. S., Blanco-Fernandez, J., Goodman, R. P., Kawakami, A., Shen, H., Kemeny, L. V., Joesch-Cohen, L., Rees, M. G., Roth, J. A., Fisher, D. E., Mootha, V. K., & Jourdain, A. A. (2023). Salvage of ribose from uridine or RNA supports glycolysis in nutrient-limited conditions. *Nat Metab*, *5*(5), 765-776. https://doi.org/10.1038/s42255-023-00774-2

Taniuchi, S., Miyake, M., Tsugawa, K., Oyadomari, M., & Oyadomari, S. (2016). Integrated stress response of vertebrates is regulated by four eIF2alpha kinases. *Sci Rep*, *6*, 32886. https://doi.org/10.1038/srep32886

Thomas, W. G., Motel, T. J., Kule, C. E., Karoor, V., & Baker, K. M. (1998). Phosphorylation of the Angiotensin II (AT1A) Receptor Carboxyl Terminus: A Role in Receptor Endocytosis. *Molecular Endocrinology*, *12*(10), 1513-1524. https://doi.org/10.1210/mend.12.10.0179

Tsitkanou, S., Della Gatta, P. A., Abbott, G., Wallace, M. A., Lindsay, A., Gerlinger-Romero, F., Walker, A. K., Foletta, V. C., & Russell, A. P. (2022). miR-23a suppression accelerates functional decline in the rNLS8 mouse model of TDP-43 proteinopathy. *Neurobiol Dis*, *162*, 105559. https://doi.org/10.1016/j.nbd.2021.105559

Vogler, T. O., Wheeler, J. R., Nguyen, E. D., Hughes, M. P., Britson, K. A., Lester, E., Rao, B., Betta, N. D., Whitney, O. N., Ewachiw, T. E., Gomes, E., Shorter, J., Lloyd, T. E., Eisenberg, D. S., Taylor, J. P., Johnson, A. M., Olwin, B. B., & Parker, R. (2018). TDP-43 and RNA form amyloid-like myo-granules in regenerating muscle. *Nature*, *563*(7732), 508-513. https://doi.org/10.1038/s41586-018-0665-2

Walker, A. K., Soo, K. Y., Sundaramoorthy, V., Parakh, S., Ma, Y., Farg, M. A., Wallace, R. H., Crouch, P. J., Turner, B. J., Horne, M. K., & Atkin, J. D. (2013). ALS-associated TDP-43 induces endoplasmic reticulum stress, which drives cytoplasmic TDP-43 accumulation and stress granule formation. *PLoS One*, *8*(11), e81170. https://doi.org/10.1371/journal.pone.0081170

Walker, A. K., Spiller, K. J., Ge, G., Zheng, A., Xu, Y., Zhou, M., Tripathy, K., Kwong, L. K., Trojanowski, J. Q., & Lee, V. M. (2015). Functional recovery in new mouse models of ALS/FTLD after clearance of pathological cytoplasmic TDP-43. *Acta Neuropathol*, *130*(5), 643-660. https://doi.org/10.1007/s00401-015-1460-x

Wang, P., Deng, J., Dong, J., Liu, J., Bigio, E. H., Mesulam, M., Wang, T., Sun, L., Wang, L., Lee, A. Y., McGee, W. A., Chen, X., Fushimi, K., Zhu, L., & Wu, J. Y. (2019). TDP-43 induces mitochondrial damage and activates the mitochondrial unfolded protein response. *PLoS Genet*, *15*(5), e1007947. https://doi.org/10.1371/journal.pgen.1007947

Wang, T., Tian, X., Kim, H. B., Jang, Y., Huang, Z., Na, C. H., & Wang, J. (2022). Intracellular energy controls dynamics of stress-induced ribonucleoprotein granules. *Nat Commun*, *13*(1), 5584. https://doi.org/10.1038/s41467-022-33079-1

Wheeler, J. R., Jain, S., Khong, A., & Parker, R. (2017). Isolation of yeast and mammalian stress granule cores. *Methods*, *126*, 12-17. https://doi.org/10.1016/j.ymeth.2017.04.020

Wickstrom, S. A., Masoumi, K. C., Khochbin, S., Fassler, R., & Massoumi, R. (2010). CYLD negatively regulates cell-cycle progression by inactivating HDAC6 and increasing the levels of acetylated tubulin. *Embo J*, *29*(1), 131-144. https://doi.org/10.1038/emboj.2009.317

Wolozin, B., & Ivanov, P. (2019). Stress granules and neurodegeneration. *Nat Rev Neurosci*, *20*(11), 649-666. https://doi.org/10.1038/s41583-019-0222-5

Xiong, X., Zhao, Y., Tang, F., Wei, D., Thomas, D., Wang, X., Liu, Y., Zheng, P., & Sun, Y. (2014). Ribosomal protein S27-like is a physiological regulator of p53 that suppresses genomic instability and tumorigenesis. *Elife*, *3*, e02236. https://doi.org/10.7554/eLife.02236

Yang, H., Sibilla, C., Liu, R., Yun, J., Hay, B. A., Blackstone, C., Chan, D. C., Harvey, R. J., & Guo, M. (2022). Clueless/CLUH regulates mitochondrial fission by promoting recruitment of Drp1 to mitochondria. *Nat Commun*, *13*(1), 1582. https://doi.org/10.1038/s41467-022-29071-4

Yu, C. H., Davidson, S., Harapas, C. R., Hilton, J. B., Mlodzianoski, M. J., Laohamonthonkul, P., Louis, C., Low, R. R. J., Moecking, J., De Nardo, D., Balka, K. R., Calleja, D. J., Moghaddas, F., Ni, E., McLean, C. A., Samson, A. L., Tyebji, S., Tonkin, C. J., Bye, C. R., . . . Masters, S. L. (2020). TDP-43 Triggers Mitochondrial DNA Release via mPTP to Activate cGAS/STING in ALS. *Cell*, *183*(3), 636-649 e618. https://doi.org/10.1016/j.cell.2020.09.020

Zaninello, M., Schlegel, T., Nolte, H., Pirzada, M., Savino, E., Barth, E., Wüstenberg, H., Uddin, T., Wolff, L., Wirth, B., Lehmann, H. C., Cioni, J.-M., Langer, T., & Rugarli, E. I. (2023). https://doi.org/10.1101/2023.12.02.569712

Zhang, K., Daigle, J. G., Cunningham, K. M., Coyne, A. N., Ruan, K., Grima, J. C., Bowen, K. E., Wadhwa, H., Yang, P., Rigo, F., Taylor, J. P., Gitler, A. D., Rothstein, J. D., & Lloyd, T. E. (2018). Stress Granule Assembly Disrupts Nucleocytoplasmic Transport. *Cell*, *173*(4), 958-971 e917. https://doi.org/10.1016/j.cell.2018.03.025

Zhao, J., Wang, X., Huo, Z., Chen, Y., Liu, J., Zhao, Z., Meng, F., Su, Q., Bao, W., Zhang, L., Wen, S., Wang, X., Liu, H., & Zhou, S. (2022). The Impact of Mitochondrial Dysfunction in Amyotrophic Lateral Sclerosis. *Cells*, *11*(13). https://doi.org/10.3390/cells11132049

Zu, T., Guo, S., Bardhi, O., Ryskamp, D. A., Li, J., Khoramian Tusi, S., Engelbrecht, A., Klippel, K., Chakrabarty, P., Nguyen, L., Golde, T. E., Sonenberg, N., & Ranum, L. P. W. (2020). Metformin inhibits RAN translation through PKR pathway and mitigates disease in C9orf72 ALS/FTD mice. *Proc Natl Acad Sci U S A*, *117*(31), 18591-18599. https://doi.org/10.1073/pnas.2005748117

Acknowledgements

This work was supported by funding provided by FightMND (IP-158) and Institute for Physical Activity and Nutrition, School of Exercise and Nutrition Sciences.